UNIVERSIDAD DE INVESTIGACIÓN DE TECNOLOGÍA EXPERIMENTAL YACHAY

Escuela de Ciencias Físicas y Nanotecnología

TÍTULO: Conductance measurements on atomic-sized contacts of gold using a low-cost mechanically controllable break junction equipment

Trabajo de integración curricular presentado como requisito para la obtención del título de Físico

Autor:

Borja Espinosa Carla Nataly

Tutor:

PhD Bramer Escamilla Werner

Co-tutor:

PhD López Alexander

Urcuquí, Junio 2020

SECRETARÍA GENERAL
(Vicerrectorado Académico/Cancillería)
ESCUELA DE CIENCIAS FÍSICAS Y NANOTECNOLOGÍA
CARRERA DE FÍSICA
ACTA DE DEFENSA No. UITEY-PHY-2020-00012-AD

A los 11 días del mes de junio de 2020, a las 15:00 horas, de manera virtual mediante videoconferencia, y ante el Tribunal Calificador, integrado por los docentes:

Presidente Tribunal de Defensa	Dr. MEDINA DAGGER, ERNESTO ANTONIO , Ph.D.
Miembro No Tutor	Dr. REINOSO CARLOS , Ph.D.
Tutor	Dr. BRAMER ESCAMILLA , WERNER , Ph.D.

El(la) señor(ita) estudiante **BORJA ESPINOSA, CARLA NATALY**, con cédula de identidad No. **0105917041**, de la **ESCUELA DE CIENCIAS FÍSICAS Y NANOTECNOLOGÍA**, de la Carrera de **FÍSICA**, aprobada por el Consejo de Educación Superior (CES), mediante Resolución **RPC-SO-39-No.456-2014**, realiza a través de videoconferencia, la sustentación de su trabajo de titulación denominado: **Conductance measurements on atomic-sized contacts of gold using a low-cost mechanically controllable break junction equipment**, previa a la obtención del título de **FÍSICO/A**.

El citado trabajo de titulación, fue debidamente aprobado por el(los) docente(s):

Tutor	Dr. BRAMER ESCAMILLA , WERNER , Ph.D.

Y recibió las observaciones de los otros miembros del Tribunal Calificador, las mismas que han sido incorporadas por el(la) estudiante.

Previamente cumplidos los requisitos legales y reglamentarios, el trabajo de titulación fue sustentado por el(la) estudiante y examinado por los miembros del Tribunal Calificador. Escuchada la sustentación del trabajo de titulación a través de videoconferencia, que integró la exposición de el(la) estudiante sobre el contenido de la misma y las preguntas formuladas por los miembros del Tribunal, se califica la sustentación del trabajo de titulación con las siguientes calificaciones:

Tipo	Docente	Calificación
Presidente Tribunal De Defensa	Dr. MEDINA DAGGER, ERNESTO ANTONIO , Ph.D.	9,7
Miembro Tribunal De Defensa	Dr. REINOSO CARLOS , Ph.D.	9,8
Tutor	Dr. BRAMER ESCAMILLA , WERNER , Ph.D.	10,0

Lo que da un promedio de: **9.8 (Nueve punto Ocho)**, sobre 10 (diez), equivalente a: **APROBADO**

Para constancia de lo actuado, firman los miembros del Tribunal Calificador, el/la estudiante y el/la secretario ad-hoc.

Certifico que *en cumplimiento del Decreto Ejecutivo 1017 de 16 de marzo de 2020, la defensa de trabajo de titulación (o examen de grado modalidad teórico práctica) se realizó vía virtual, por lo que las firmas de los miembros del Tribunal de Defensa de Grado, constan en forma digital.*

BORJA ESPINOSA, CARLA NATALY
Estudiante

Dr. MEDINA DAGGER, ERNESTO ANTONIO , Ph.D.
Presidente Tribunal de Defensa

Firmado electrónicamente por:
ERNESTO ANTONIO
MEDINA DAGGER

Dr. BRAMER ESCAMILLA , WERNER , Ph.D.
Tutor

Firmado electrónicamente por:
WERNER
BRAMER

Dr. REINOSO CARLOS , Ph.D.
Miembro No Tutor

CIFUENTES TAFUR, EVELYN CAROLINA
Secretario Ad-hoc

AUTORÍA

Yo, **CARLA NATALY BORJA ESPINOSA**, con cédula de identidad 0105917041, declaro que las ideas, juicios, valoraciones, interpretaciones, consultas bibliográficas, definiciones y conceptualizaciones expuestas en el presente trabajo; así cómo, los procedimientos y herramientas utilizadas en la investigación, son de absoluta responsabilidad de el/la autora (a) del trabajo de integración curricular. Así mismo, me acojo a los reglamentos internos de la Universidad de Investigación de Tecnología Experimental Yachay.

Urcuquí, julio 2020

_____
Carla Nataly Borja Espinosa
CI: 0105917041

AUTORIZACIÓN DE PUBLICACIÓN

Yo, **CARLA NATALY BORJA ESPINOSA,** con cédula de identidad 0105917041, cedo a la Universidad de Investigación de Tecnología Experimental Yachay, los derechos de publicación de la presente obra, sin que deba haber un reconocimiento económico por este concepto. Declaro además que el texto del presente trabajo de titulación no podrá ser cedido a ninguna empresa editorial para su publicación u otros fines, sin contar previamente con la autorización escrita de la Universidad.

Asimismo, autorizo a la Universidad que realice la digitalización y publicación de este trabajo de integración curricular en el repositorio virtual, de conformidad a lo dispuesto en el Art. 144 de la Ley Orgánica de Educación Superior

Urcuquí, julio 2020

_____
Carla Nataly Borja Espinosa
CI: 0105917041

Dedicatoria

A mis sobrinos Nicolás, Valentina y Juliana, que con sus abrazos, alegría, e inocencia muchas veces reavivaron mi espíritu.

Carla Nataly Borja Espinosa

Agradecimientos

Resumen

El montaje experimental de la unión de ruptura controlable mecánicamente (MCBJ) es una de las principales técnicas empleadas en el estudio de las propiedades de transporte electrónico a escala nanométrica. Este trabajo presenta la construcción de un equipo innovador, robusto, de bajo costo, y simple que permite observar la cuantización de la conductancia a medida que un cable de oro macroscópico se estira hacia dimensiones atómicas. El equipo hecho a mano se basa en el principio de la técnica MCBJ y permite formar y romper un contacto metálico continuamente para realizar un análisis estadístico de los datos. El histograma construido a partir de mediciones de conductancia a temperatura ambiente en aire, muestra que la calidad del equipo MCBJ construido es comparable a la calidad de un equipo similar utilizado en laboratorios de investigación. El equipo es capaz de resolver hasta el tercer pico que caracteriza el histograma de conductancia de nanocables de oro reportado en la literatura. Se sugiere que dicho experimento se implemente como una poderosa herramienta pedagógica en clases de física contemporánea.

Palabras clave: cuantización de la conductancia, contacto de oro de tamaño atómico, unión de ruptura controlable mecánicamente, microscopio de efecto túnel.

Abstract

The mechanically controllable break junction (MCBJ) experimental setup is one of the main techniques employed in the study of electronic transport properties at the nano-scale. This work presents the construction of an innovative, robust, low-cost, and simple equipment that shows the emergence of conductance quantization as a macroscopic gold wire is pulled up to atomic dimensions. The handmade equipment is based on the MCBJ principle and allows forming and breaking a metallic contact continuously to perform a statistical analysis of the data. The histogram built from conductance measurements at room temperature in air, shows that the quality of the built MCBJ equipment is comparable to that of a similar equipment used in research laboratories. It is able to resolve up to the third peak that characterizes the conductance histogram of gold nanowires reported in the literature. Such an experiment is suggested to be implemented as a powerful pedagogical tool in lectures of contemporary physics.

Keywords: conductance quantization, atomic-sized gold contact, mechanically controllable break junction, scanning tunneling microscope.

Contents

List of Figures

Chapter 1

Introduction

In an attempt to understand matter properties and quantum mechanical effects that arise as size is reduced down to the nanoscale, electrical conduction in atomic-sized metallic contacts has been widely studied in a theoretical and experimental context[1]. An atomic-sized contact or nanocontact is a local point of contact between two macroscopic conductors, where the electrical current is constrained to pass through a cross-section of about a nanometer. Interesting properties arise in this scenario leading to new technological implementations. In particular, it has been proposed to use single-atom contacts as quantized resistors, capacitors[2], or switches[3]. Another useful application is to fabricate nanoelectrodes to connect single molecules and characterize the electronic transport through them to be incorporated in molecular devices[4,5]. Nanowires are also useful as chemical sensors due to their sensitivity to the adsorption of molecules[6].

The Scanning Tunneling Microscope in the break junction regime (STM-BJ) and the Mechanically Controllable Break Junction (MCBJ) are the main experimental techniques used to manipulate and characterize the electronic and mechanical properties of nanocontacts[1]. Briefly, after the invention of the STM in 1986, Gimzewski and Moller were the first to employ an STM to study the electrical conductivity in atomic-sized metallic contacts[7]. They investigated the dynamics of the transition from tunneling to contact regime by monitoring the current in the system during subsequent variations of the tip-sample distance in an STM. Later in 1992, in Leiden, Muller et al.[8] introduced a new technique focused on studying atomic-sized point contacts, named Mechanically Controllable Break Junction (MCBJ), whose principle consists of pulling a macroscopic metal wire

with a narrow section, neck or constriction. During elongation, the strain is concentrated at the weak spot that the narrow section represents, and it ends up forming a thin contact, sometimes with the width of a single atom, before eventually breaking. Using fine control for the rupture by means of piezoelectric materials, atomic-sized contacts can be formed and broken many times. The MCBJ technique has better mechanical stability and is less prone to atmospheric contamination in comparison with the STM-BJ[9]. An improved MCBJ model, was introduced by Zhou et al. in 1995[10]. It has the same principle as the original model but employs a freely-suspended bridge in a thin metal film produced by standard electron-beam lithography instead of a neck-shaped wire. This design provides the junctions with high insensitivity to external mechanical perturbations as a result of the smaller ratio between the piezo displacement and the gap electrode size.

Experiments performed with the referenced techniques show that the conductance in atomic-sized metallic contacts decreases in a step-wise manner as the width of the contact decreases[11–15]. By constructing histograms from the accumulated count of conductance values during several cycles of rupture and formation of the metallic contact, it was observed that the conductance has certain preference for integer multiples of the quantum of conductance denoted as $G_0 = 2e^2/h$ where e is the electron charge and h is the Planck's constant. This phenomenon of conductance quantization arises because of the wave-particle characteristics of electrons. The distance an electron travels between two scattering events, known as the mean free path, is typically much larger than the atomic size. However, when the dimensions of the conductor are reduced and become comparable to the de Broglie wavelength of the electrons at the Fermi surface, electrons can traverse the conductor ballistically. In addition, the radial confinement provided by the small width of the conductor allows just a finite number of wavelengths or conduction channels being accessible, forming a discrete set of one-dimensional energy bands that depends on the width of the conductor. Thus, as the width of the conductor gets narrower, the number of available conduction channels reduces and the conductance decreases in steps of the order of the quantum of conductance[16].

The focus of this work is the construction of a low-cost MCBJ setup to measure electronic transport through atomic-sized contacts of gold at room temperature and ambient conditions. The obtained results will be compared with the measurements taken in the "Laboratorio de Bajas Temperaturas y Sistemas Nanométricos" LT-NanoLab of the University of Alicante in Spain in collaboration with professors Ph.D. Carlos Sabater and Ph.D. Carlos Untiedt using STM-BJ equipment fabricated by their group. The sections below are structured as follows. Chapter 2 covers the theory that describes the electronic transport in atomic-sized contacts. It also explains the experimental methods to fabricate these atomic contacts and how to analyze and interpret the results. Next, Chapter 3 shows the design and operating principle of the MCBJ equipment built for this work. Chapter 4 presents the analysis of measurements performed with the built MCBJ and the comparison with the results obtained using the STM-BJ technique. Finally, the most relevant processes and outcomes, as well as recommendations for future work, are summarized in Chapter 5.

1.1 Problem Statement

Electronic transport at the nanoscale leads to quantum effects such as the quantization of conductance. This phenomenon is a main subject in mesoscopic physics and it is important to be understood for the proper design of new electronic devices. Direct observation of this quantum effect during experiments can motivate a good perception and basic understanding of the phenomenology of quantum transport. How to address this pedagogical interest, without requiring an expensive investment, and in a way that can be easily conducted by undergraduate students? In answer to this question, the present work describes the assembly of an innovative, robust, low-cost, and simple equipment to measure conductance through atomic-sized contacts of gold, and obtain statistical information of the experimental data. This setup allows the user to observe conductance quantization in real time. On the other hand, it also involves activities and concepts such as trigger-

ing, data acquisition and selection, and noise analysis. It can be highlighted with certainty that this equipment is the first of its kind developed in Ecuador and in general, it employs a MCBJ technique never used before, based on the vibrations of a loudspeaker. It represents a powerful pedagogical tool that motivates future projects related to the electronic transport on metallic and molecular nanocontacts within Yachay Tech University and hopefully, it can inspire other institutions in the country to build similar devices.

1.2   General and Specific Objectives

General Objective

- Construction of an innovative, robust, low-cost, and simple MCBJ equipment based on the vibrations of a loudspeaker.

Specific Objectives

- To build the mechanical structure of the MCBJ equipment using a loudspeaker to control the formation of atomic-sized contacts.

- To prepare the circuit and connections of the MCBJ equipment to measure and acquire the data trying to get the highest resolution and lowest possible noise.

- To perform an statistical analysis of conductance values measured during consecutive cycles of junction/breaking of atomic-sized contacts.

- To compare measurements performed by research level STM-BJ equipment, built in the 'Laboratorio de Bajas Temperaturas y Sistemas Nanométricos' of the University of Alicante, and the MCBJ equipment built at Yachay Tech.

Chapter 2

Theoretical Background

2.1 Electronic transport in metallic point contacts

This section reviews the basic theory of electronic transport on small conductors. Particularly, it includes a complete derivation of the conductance in the scattering approach. Such description, pioneered by Landauer, applies in the case of atomic-sized contacts. In the process, references[16,17] will be mainly used.

Consider a macroscopic wire with a constriction of width w and length L. The conductance of this system depends on the relative sizes of w and L compared to the mean-free-path l, which is defined as the average distance that the electrons travel between successive collisions with the lattice, and the de Broglie wavelength at the Fermi surface λ_F of the electrons in the wire. Figure 2.1 represents the transport regimes that produce different conduction properties across the constriction.

The classical limit or diffusive regime is defined when w and L are much larger than the mean-free-path. Therefore, an electron traveling through the constriction will scatter many times with high probability before it reaches the end of the constriction (see Figure 2.1(a)). In this case, the conductance is given by the following expression known as the Maxwell conductance[19]

$$G = 2w\sigma. \tag{2.1}$$

where σ is the conductivity of the material. Thus, in the classical limit, the conductance is a smooth function of the radius of the constriction, which applies to macroscopic conductors.
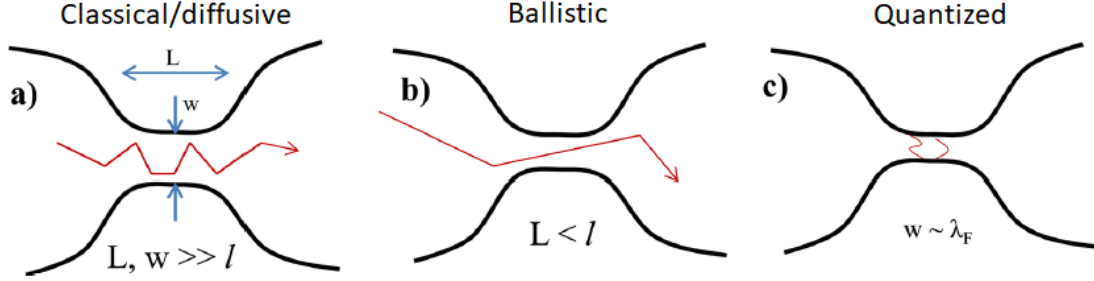
Figure 2.1: Representation of the different transport regimes that characterize the conduction on a wire with a constriction of length L and width w. Retrieved from[18].

On the other hand, when the length of the constriction is smaller than the mean-free-path $L < l$, the regime is named ballistic. Here, the electrons will pass through the constriction with no momentum loss and only limited by scattering with the boundaries, as shown in Figure 2.1(b). The conductance in this limit is known as the Sharvin conductance and is given by[20]

$$G = \frac{2e^2}{h} \left(\frac{k_F w}{2} \right)^2.$$ (2.2)

where h is Planck's constant, k_F is the wave vector at the Fermi energy, and w is the constriction width. The conductance in this limit is independent of the material conductivity and increases quadratically with the width of the constriction.

Finally, if the constriction radius continues to shrink down to the atomic scale, it will be comparable to the Fermi wavelength $w \approx \lambda_F$. The conductance in this limit is quantized, and the radial confinement will allow only a finite number of wavelengths or conduction channels to be transmitted (see Figure 2.1(c)). The expression of the conductance in this regime is derived below following the scattering approach of Landauer[21].

Quantum Limit

By definition, the conductance is given in terms of the current and potential difference as

$$G = \frac{I}{V}. \tag{2.3}$$

where I is the current and V the potential difference across the sample. A classical approach is to consider the charge motion as a response to an applied electric field with its associated gate voltage. The remarkable idea of Landauer was to approach the electron transport as a transmission process, i.e., as a scattering problem where the current is associated with charge transmission across a scattering barrier. Hence, the electrical current is measured in terms of the probability that charge carriers reach the drain from the source. This approach has shown to be extremely useful to describe the transport properties of nanostructured devices, ranging from metallic to molecular systems[17]. The following derivation gives the main ingredients for understanding the problem under consideration.

Consider two wide electron gas reservoirs with respective chemical potentials μ_1 and μ_2 connected by an ideal (no dissipation) conductor of width w and length L (see Figure 2.2(a)). The conductor is infinitely long in the x-axis (direction of net electron flow) and has a small width (less than 1nm) in the transverse direction ($w \ll L$), comparable in size to that of the Fermi wavelength $w \approx \lambda_F$, and L being smaller than the mean-free path of electrons ($L < l$). Under these conditions, the electrons are only scattered by the boundaries of the conductor and can move ballistically between the two reservoirs. Furthermore, due to the transverse confinement, only a finite number of wavelengths or "conduction channels" are allowed in the transverse direction[18].

The electron dynamics inside the conductor is described by the Schrödinger's eigenvalue equation[16]

$$\left(\frac{-\hbar^2 \nabla^2}{2m} + U(y, z) \right) \psi(x, y, z) = E\psi(x, y, z). \tag{2.4}$$

where m is the electron's mass, $U(y, z)$ is the potential energy in y and z, implying free diffusion
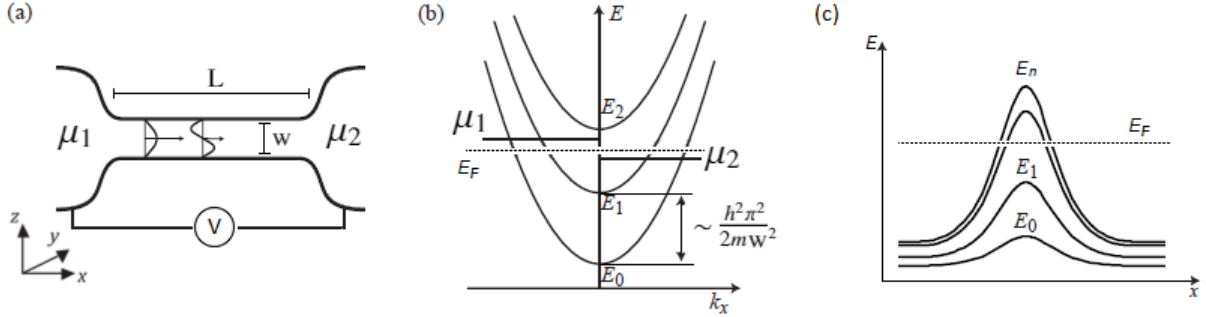
Figure 2.2: Quantized conductive channels in a nanowire. (a) Representation of a nanowire of length L and width w connecting two electron reservoirs with chemical potentials μ_1 and μ_2. The wave function profiles of the available transverse modes are represented within the conductor. (b) Dispersion relation of the transverse modes. The energy splitting between the subbands depends on the width of the conductor. (c) The electrons flowing through the nanowire see a potential barrier. Only the modes with a barrier less than the Fermi level of the conductor E_F contribute to the conductance. Adapted from [22].

along x. Due to the dimensions of the conductor ($w \ll L$), it can be treated in good approximation as being translational invariant in the x-direction, so it is possible to use the separating ansatz [16]

$$\psi(x,y) = exp(ik_x x)\chi_n(y,z). \tag{2.5}$$

where $\chi_n(y,z)$ are the *transverse modes* of the wire and *n* is the index for the discrete spectrum. Assuming a parabolic confinement in *y* and *z*, the energy of the electrons in the conductor can be written as [16,23]

$$E_n(k) = \frac{n^2\hbar^2\pi^2}{2mw^2} + \frac{\hbar^2 k_x^2}{2m}. \tag{2.6}$$

This equation describes *n* parabolic subbands in k-space with energy spacing that depends on the width of the conductor (see Figure 2.2(b)). The electrons flowing through the nanoconductor see an effective potential energy and only the modes with a barrier less than E_F will be perfectly

transmitted (see Figure 2.2(c)). As the width of the conductor decreases, the energy subband spacing will be larger and therefore, the number of discrete available levels that lie below the Fermi energy decreases. The total current is given by the sum of the microscopic currents of all the subbands or transverse modes. Thus, **as the width of the conductor gets tighter, the conductance will decrease in a step-like manner**[1,16,23].

Under a bias voltage the chemical potential of each reservoir is shifted, and a net current starts to flow. The electrons are driven from source to drain via the potential difference $V = (\mu_1 - \mu_2)/e$, with $\mu_1 > \mu_2$, and e being the electronic charge. Considering a perfectly transmitted mode, the net current is equal to the difference of particles flowing from the left and right reservoirs[17], i.e.

$$I = e \int_0^\infty dk v(k) \left(n_1(k) - n_2(k) \right),$$ (2.7)

where $v(k)$ and $n_1(k), n_1(k)$ are the group velocity and the one-dimensional density of states for the left and right reservoirs respectively, defined as[17]:

$$v(k) = \frac{1}{\hbar} \frac{dE_n(k)}{dk} = \frac{\hbar k}{m},$$ (2.8)

$$n(k) = \frac{1}{\pi} f(E_k),$$ (2.9)

which the latter includes degeneracy of the spin and is multiplied by the Fermi-Dirac distribution. Replacing equations 2.8 and 2.9 in 2.7 leads to

$$I = e \int_0^\infty dk \frac{\hbar k}{m} \frac{1}{\pi} \left(f_1(E_k - \mu_1) - f_2(E_k - \mu_2) \right),$$ (2.10)

The resulting current I through the nanoconductor is carried by the uncompensated states in the energy interval defined by μ_1 and μ_2. In the limit of low temperature and small voltage, i.e., when the thermal energy $k_B T$ and gate voltage eV, where $k_B T$ is the Boltzmann's constant and T the absolute temperature, are much smaller than the subband splitting, the Fermi level of each reservoir is approximately equal to μ_1 and μ_2, and $f_1(E_k - \mu_1), f_2(E_k - \mu_2)$ are step functions equal to 1 below

$E_F + eV/2$ and $E_F - eV/2$, respectively, and 0 above this energy. Then, writing Eq. 2.10 in the energy domain and using Eq. 2.8 results in

$$
\begin{aligned}
I &= \frac{e}{\pi}\frac{\hbar k}{m} \int_{\mu_2}^{\mu_1} dE\,\frac{dk}{dE}, \\
I &= \frac{e}{\pi}\frac{\hbar k}{m}\frac{m}{\hbar^2 k} \int_{\mu_2}^{\mu_1} dE, \\
I &= \frac{2e}{h}(\mu_1 - \mu_2), \\
I &= \frac{2e^2}{h}V.
\end{aligned}
$$

Finally, using the definition of conductance $G = I/V$, it leads to the compact result

$$
G = \frac{2e^2}{h} = G_0. \tag{2.11}
$$

Then, if the energy spacing between the transverse modes is significantly larger than $k_B T$ and for a small voltage $eV << k_B T$, the conductance varies in steps of the quantum of conductance G_0, that has the numerical value $G_0 \approx (12,9k\Omega)^{-1}$ or $77.48\mu S$ [22], with each additional occupied mode. In metals, the splitting between the quantum modes is in the order of $\pi^2\hbar^2/2m\lambda_F^2 \approx 1\ eV$ ($\lambda_F = 0.5$ nm for gold), which is high enough for detection of quantum behavior at ambient temperature [1,23]. In general, the system is not ideal and thus 100% transmission probability is not possible due to scattering with impurities that are typically present in the space separation. Therefore, the conductance for N transverse modes with transmissions $T_i(E_F)$ is [22]

$$
G = \frac{2e^2}{h}\sum_{i=1}^{N} T_i(E_F). \tag{2.12}
$$

Tunneling current

Another transport property that arises during the formation of atomic-sized contacts is the conduction of the electrons through a vacuum gap when the two electrodes are a few angstroms

($\mathring{A} = 10^{-10}$m) apart. In this situation, once they are connected to a voltage supply, even though they are not in contact, electrons start to flow. The origin of this current is explained by the tunnel effect which consists on the no null probability that an object has to cross a potential barrier of energy greater than itself due to its wave-particle properties. This tunnelling current can be expressed by the following proportionality relationship:

$$I \propto e^{-\frac{\sqrt{2m\phi}}{h}d}.$$ (2.13)

This expression shows the relation between the current I and the distance d that separates the electrodes, where m is the electron mass, h is the Planck constant and ϕ is the work function of the metal. According to this expression, the tunneling current decays exponentially as the separation between the electrodes increases. For common metals the work function is in the order of $\phi \approx 4eV$ so the tunneling current varies in one order of magnitude when the distance between electrodes changes approximately in 1$\mathring{A}$.

2.2 Fabrication of metallic point contacts

2.2.1 Requirements of the experimental setup

As reviewed in section 2.1, quantization of conductance is observed during electronic transport in the constriction of a metallic wire whose dimensions are comparable to the mean-free-path of the electrons and the Fermi wavelength. Costa et al.[24] showed that it is possible to measure conductance quantization when two macroscopic wires touch each other slightly by vibrating in and out of contact and using an oscilloscope. However, to obtain more reliable results and enough statistical information, it is necessary to separate or approach two electrodes in a controlled manner with micro or nanometer precision to form a connecting neck of variable cross-section. This fine control is possible using piezoelectric materials, which can move in the range of nanometers when a

high voltage is applied to them[9]. The conductance measurements will be independent of the initial size and shape of the contact between the electrodes. Thus, macroscopic or microscopic wires at different configurations can be used to form nanocontacts[24].

   To measure the conductance, one of the electrodes that forms the gold atomic-sized contact is connected to a constant bias voltage, and the current signal from the other electrode goes to a low noise trans-impedance amplifier or I/V converter which main component is an operational amplifier (op-amp). The I/V-converter amplifies and converts the current into voltage to be read by a fast digital oscilloscope or a digital analogical converter (DAC). Other form to measure the resistance variations in the constriction is to measure the voltage drop across a current-sensing resistor connected in series with the constriction[25]. The employed general circuit is shown in Figure 2.3. Note that during approaching or separating the electrodes, the contact size changes constantly implying different resistances. Therefore, the constriction in the wire essentially represents a variable resistor.
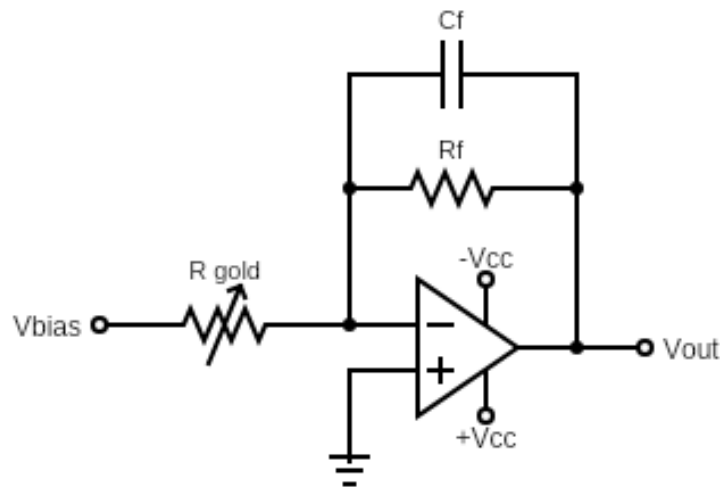
Figure 2.3: General circuit used to measure the conductance through atomic-sized contacts where the gold constriction is represented as a variable resistor. Adapted from[9].

As shown in Figure 2.3, the op-amp is in the negative feedback mode, so the differential input voltage is kept at 0 V with the right electrode virtually connected to ground. No current flows into the inverting input of the op-amp, so it goes entirely through the feedback resistor R_f, which sets the gain of the op-amp given in voltage per ampere (V/A). The value of the voltage supply $\pm V_{CC}$ that feeds the op-amp limits the maximum output voltage from it. Using a negative bias, the relation between the input current I that comes from the gold constriction, and the output voltage V_{out} from the op-amp, is given by[26]

$$V_{out} = R_f I,\tag{2.14}$$

where R_f if the feedback resistor. Using Ohm's law, this output voltage can be transformed into the conductance through the gold constriction G_{gold}, with the following relation:

$$G_{gold} = \frac{1}{R_{gold}} = \frac{V_{out}}{R_f\,V_{bias}}.\tag{2.15}$$

which can be expressed in units of the conductance quantum normalizing by the value $G_0 = 12.9\,k\Omega$.

The presence of a feedback capacitor C_f connected in parallel with the feedback resistor maintains the stability of the amplifier. It also limits the frequency response since the output gain of signals with frequencies higher than the bandwidth of the amplifier will be reduced. The upper cutoff frequency or bandwidth is given by the expression

$$f = \frac{1}{2\pi C_f R_f}.\tag{2.16}$$

Experiments for recording the conductance on atomic-sized contacts are performed under HV or UVH conditions to isolate the sample from the environment. Contamination from adsorbates or oxides avoid the formation of nanocontacts and alter the results. The temperature also influences the results and generally is preferred to work at low temperatures to minimize the kinetic energy of the system and favor the formation of mechanically stable structures[9].

The next section describes the characteristics and operation of the two main experimental techniques used to fabricate metallic atomic-sized contacts and study them through electronic

transport measurements. These are the Scanning Tunneling Microscope Break Junction (STM-BJ) and the Mechanically Controllable Break Junction (MCBJ).

2.2.2   Scanning Tunneling Microscope Break Junction (STM-BJ)

The Scanning Tunneling Microscope Break Junction (STM-BJ) technique creats atomic-sized contacts by indenting and retracting the tip of an STM to and from a metallic surface, as shown in Figure 2.4. During each indentation, the conductance reaches a value 10 to 40 times greater than the quantum of conductance. This electric force restructures the shape of the electrodes with every indentation. Then, upon retraction, a nanowire is formed that thins down until it breaks[27]. Ramps of high voltage (± 15 V) at the piezopiles of the STM control the process of indentation and retraction with nanometric precision.
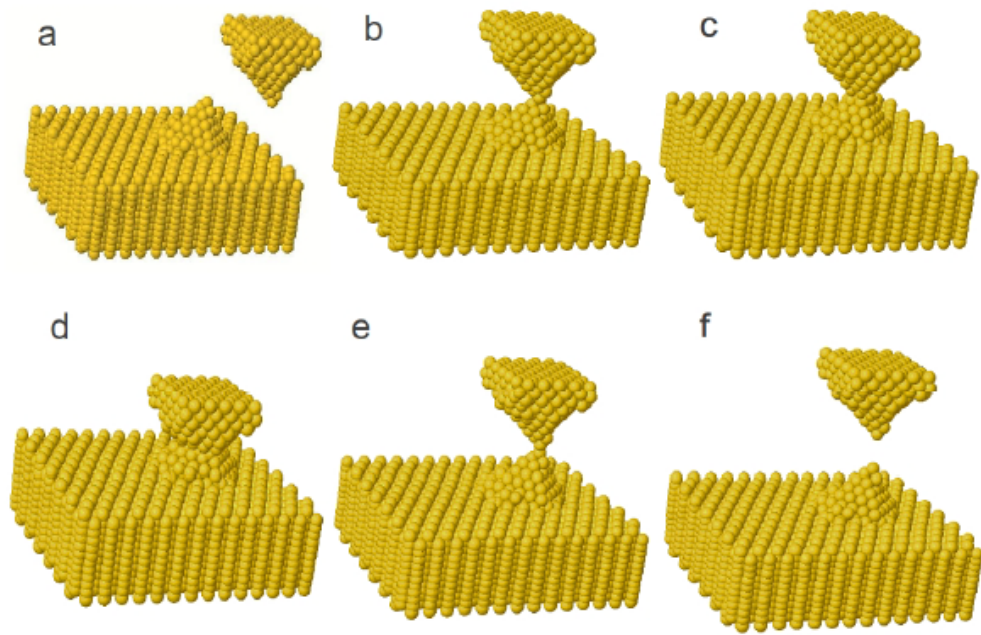
Figure 2.4: Procedure to create a nanocontact using an STM. Retrieved from[9].

The mechanism for the formation of nanowires is explained by the cohesive bonding between the tip and the sample. Upon subsequent tip retraction, in the case of clean metallic contacts, the atoms from the tip and the sample form a neck of the material which breaks, leading to a localized protrusion. On the contrary, in the presence of contamination, such cohesive bonding is much weaker, which causes the forces from the tip to be inefficient to pull material from the surface and form nanowires[7].

STM conductance experiments have been performed at low[11,28] and room temperature under UHV[12,15,29] and ambient conditions[14,30]. In situ cleaning procedures for the tip and the sample are used under UHV conditions. On the other hand, at ambient conditions, it is possible to obtain fresh and clean surfaces after several cycles of rupture-formation while making deep tip-surface indentations to rearrange the atoms and remove oxides[7].

2.2.3   Mechanically Controllable Break Junction (MCBJ)

For the technique called MCBJ, the metallic sample under consideration is a notched-wire or a wire with a constriction. The constriction or the notch in the wire can be cut manually to a diameter about one-third of the original wire by rolling the metal under the tip of a surgical knife. As shown in Figure 2.5, this notched-wire is then fixed onto a flexible insulating substrate by applying two drops of epoxy adhesive at each side of the constriction, defining a distance u between them. The constituting material of the substrate is usually phosphorous bronze, silicon, or spring steel, and to insulate its surface, this is covered with a film of Kapton polyimide. Finally, the whole structure is mounted in a three-point bending configuration with a stacked piezo in the central part and two fixed lateral supports separated by a distance L.

To form the nanowires, the substrate is bent progressively by moving forward the piezo. The strain is concentrated at the weak spot created by the notch (section 'u' in Figure 2.5), resulting in continuous stretching of the notched section until it breaks forming atomic-sized contacts with clean
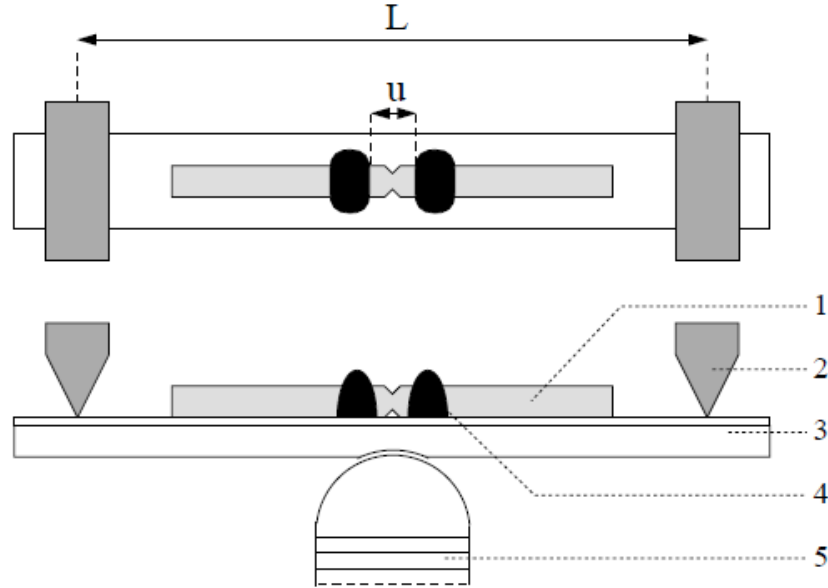
Figure 2.5: Schematic top and side view of the mounting of a MCBJ, with the notched wire (1), two fixed counter supports (2), bending beam (3), drops of epoxy adhesive (4) and the stacked piezo element (5). Retrieved from [1].

surfaces at the last stages of the rupture. By relaxing the force on the substrate, the two atomic-sized facing electrodes, simultaneously generated during the breaking, start to approach each other recovering the original wire. By means of the stacked piezo control, atomic size contacts can be reformed and broken many times [27].

Because of the three-point bending mechanical configuration, the vertical motion of the push piezo (Δz) causes a highly reduced horizontal displacement (Δx) of the electrodes. Considering the ideal case of homogeneous strain in the substrate, the ratio between (Δz) and (Δx), known as the attenuation factor, is calculated as [31]:

$$r = \frac{\Delta x}{\Delta z} = \frac{6ut}{L^2}. \tag{2.17}$$

where t is the thickness of the substrate, u is the length of the constriction in the wire and L

is the distance between the two lateral supports. A small displacement ratio reduces undesired mechanical effects from external vibrations, thermal expansion or voltage instability on the piezo element[31].

The hand-operated mechanical notching electrodes are the simplest ones employed in a MCBJ set-up and have the advantage that can be easily adapted to almost all metal electrodes. With the development of lithography techniques, new generations of MCBJ appeared. For example, electrodes are also fabricated through electrochemical deposition on the basis of optical lithography[32] or using E-beam lithography and reactive ion etching[33], which are sophisticated and advanced techniques[34]. One of the advantages of using lithographic techniques is an improved insensitivity to external mechanical perturbations as a result of their displacement ratio two orders of magnitude smaller than for a regular device.

The main advantage of the MCBJ over the STM-BJ is its higher mechanical stability in the whole temperature range. This is because the electrodes are rigidly fixed at a small separation, so the cycle of rupture-formation of the contact takes less mechanical effort in comparison with the STM-BJ technique[1]. As a consequence, disturbing factors such as external vibrations, thermal drifts, and discontinuous motion of the piezo-element can be almost ignored, especially in the low-temperature regime[35]. Another advantage of the MCBJ is that, during the breaking process, two clean fracture surfaces are generated in situ and, under controlled conditions without pollutant particles, the influence of contaminants is minimized[1]. In contrast, when using an STM, the samples are prepared in room conditions, and in situ cleaning procedures are necessary. Additionally, the MCBJ can be conveniently integrated with other systems, such as inelastic electron tunneling spectroscopy, surface-enhanced Raman scattering, and electrochemical deposition[35]. However, one of the principal drawbacks of the MCBJ is that it is not possible to have details of the contact geometry; the exact shape and atomic configuration of the electrodes are always uncertain[31].

2.3   Methods for the data analysis

This section explains the basic methodologies used for the analysis of conductance measurements obtained from the electronic transport in atomic-sized contacts independently of the experimental setup.

2.3.1   Traces of conductance

The conductance during the formation of atomic-sized contacts is recorded as a time function. It can also be represented as a function of the voltage ramps applied to the piezopiles of the STM or the relative displacement between the electrodes. Figure 2.6 shows a typical trace of conductance. The down arrow points how the conductance decreases in a step-wise manner as the electrodes get apart down to the value of one quantum of conductance G_0 followed by a abrupt jump out of contact when the contact breaks. On the other hand, the up arrow indicates the movement of contact formation. In the zone between 0 and 1 G_0 before contact, the conductance increases exponentially as expected for vacuum tunneling (equation 2.13). Later, the conductance jumps and starts to increase in a step-wise manner as the electrodes get closer.

Conductance traces show plateaus which are nearly flat for the lowest conductance values or small size contacts and plateaus with a negative inclination for the opposite case (high conductance or large size contacts). After each plateau, an abrupt jump in the order of the conductance quantum unit G_0 is observed. However, the coincidence of the plateaus with multiples of G_0 is not perfect. This is because, the nature of the sharp steps in the conductance does not result directly from quantization and does not depend exclusively on the narrowest cross-section of the contact.

Simultaneous measurements of forces and conductance,[36–38] and analogous molecular dynamics simulations[39,40] show that sudden structural atomic-scale rearrangements of the nanocontact, that lead to stress relaxation, are the fundamental cause of the abrupt jumps in the conductance.
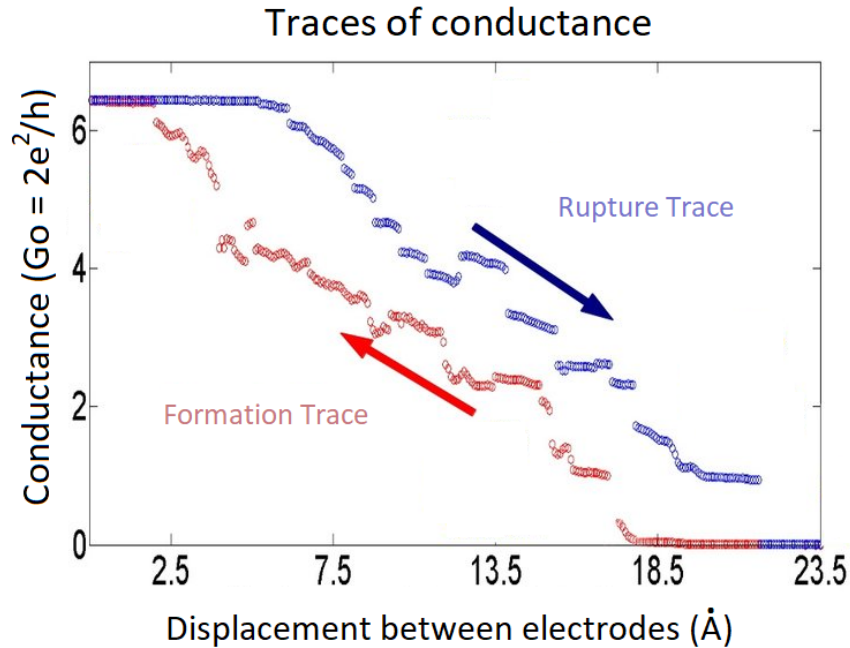
Figure 2.6: Variation of the conductance for the process of rupture and formation of an atomic-sized contact. Adapted from[9].

Figure 2.7 shows the evolution of force and conductance measured simultaneously. During the indented sections of the force curve, the contact deforms elastically until it becomes unstable and suddenly relaxes by changing its structure. This new arrangement differs on one atomic spacing from the previous one[1]. The previous result also shows that during the elastic deformations of the contact, the conductance is relatively stable and changes suddenly at the same time that a different system configuration is established. In other words, the contact goes through a sequence of discrete stable atomic configurations that represent a local energy minimum, which changes abruptly as a result of the induced stress[1].

The number of available conductance channels on monoatomic contacts is determined by the chemical nature of the metal. Tight binding calculations[41] of metallic one-atom contacts predict a
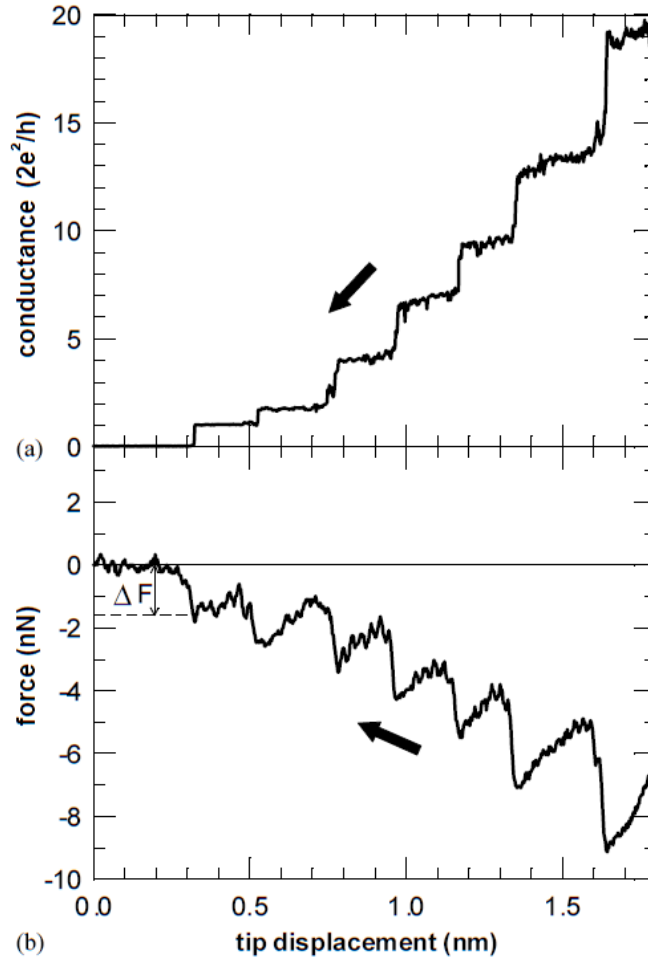
Figure 2.7: Simultaneous conductance (a) and force (b) measurements in a nanocontact at 300 K. Adapted from[36].

fully open single conduction mode, for monovalent metals like gold where the s-electrons dominate the density of states at the Fermi energy, and it contributes ~ 1 G_0 to the conductance, which means that the conductance plateau near 1 G_0 represents a contact of monoatomic size. Therefore, in the case of monovalent metals, as the contact varies its structure by one atomic spacing, the channels will be opened or closed one by one, revealing the quantum nature of conduction.

Perfect quantization favors when the contact, apart from having a length and width shorter than the electron mean-free-path, it also has a cross-section that varies slowly with the longitudinal coordinate, which corresponds to a small opening angle at the leads[42]. In this case, the oscillations in the force, and the variations in the conductance due to the opening or closing of a transmission channel are synchronized. Whereas in a more realistic geometry, the contact size does not vary smoothly and quantum effects cannot be directly observed. Another factor that influences conductance quantization is the matching between the atomic wave functions in the contact and the wave functions in the leads. If they are not perfectly coupled, the quantum channels will not be entirely transmitted[11]. In addition, the effects of surface roughness, adsorbates, and large opening angles of the leads cause backscattering that destroys conductance quantization and deviate the position of the plateaus from integer values[29,43–45].

Note also that conductance traces are different from each other since the sequence of contact structural rearrangements is different during each cycle of rupture-formation. However, the mechanical properties of the constriction may lead to specific preferred geometries, especially for the first and last atomic contacts, which represent the lowest two or three conductance plateaus. Thus, some values of conductance may occur more often than others, also because a wide range of constriction geometries may correspond to the same conductance[11,46].

2.3.2   Histograms of conductance

To perform an objective analysis of the preferential conductance values, a large number of individual curves of contact breaking are collected and plotted as histograms. Assuming that the experimental recording cycles are slow in comparison with the atomistic relaxation rates, the junction has enough time to relax into a set of particularly stable junction geometries. Therefore, considering that all possible configurations are equally likely to be formed, the peaks in the histogram are interpreted as representing the most favorable energetically junction configurations preferred by the electronic

system and the height of the peaks indicates which structures are the most stable[27]. Since several thousands of curves are usually necessary for a better resolution of the smaller peaks[47], the cycles of rupture-formation are carried out in a time in the order of a second or shorter.

An example of a conductance histogram for gold is shown in Figure 2.8. It shows that conductance has a predilection for integers of G_0. One principally observes peaks near 1, 2, and 3 G_0. Sometimes also broad peaks form at 4 and 5 G_0[48]. At 4.2 K and HV conditions, authors from reference[28] found peaks centered at 0.97 ± 0.07, 1.7 ± 0.2, and 2.7 ± 0.2, which vary slightly towards higher values at room temperature. The first peak is always sharp, higher than the others, and in the range between 0.8 G_0 and 1.2 G_0.
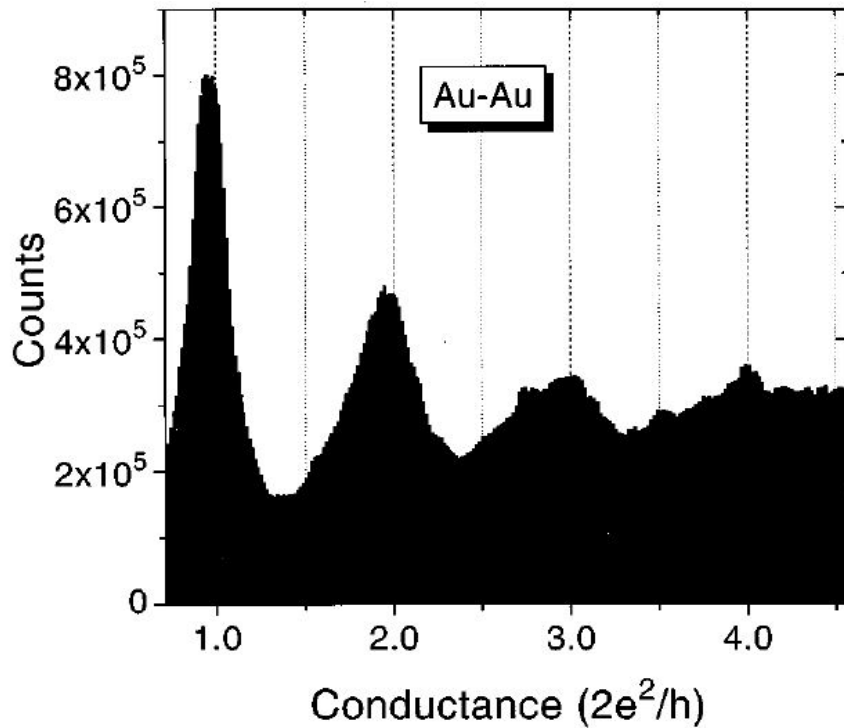

Figure 2.8: Conductance histogram for gold built with 18000 consecutive contact breakage experiments recorded using an STM at room temperature in air. Retrieved from[49].

Effect of different experimental conditions

The distinct features in the histogram of gold are very robust and almost independent of temperature, environment, and experimental technique. When working with other metals, the experiment requires vacuum or liquid-helium conditions to obtain reproducible results[46]. This characteristic property of gold is attributed to its inert surface and easy cleaning process. However, considerable variations of the bias voltage or speed of retraction influence the histogram peaks as described below. Even the environment (air or vacuum) and temperature conditions affect the form of the histogram, although no in a significant way.

The gold conductance histogram peaks decrease in height while the bias voltage increments until they vanish[25,50]. The first peak around 1 G_0 is very robust. At room temperature, it remains almost unchanged up to a bias voltage of 1.0 V. It starts to decrease at 1.5 V and finally disappears at 1.9 V, which is equivalent to a maximum current of 137 μA. This value changes slightly to 2.2 V and 165 μA at low temperatures. Likewise, the peaks above 1 G_0 start to decrease at 1.0 V. They all disappear at 1.5 V. Finally, at 2.0 V, the histogram shows no peak structures. This behavior is because high current density induces electromigration of the atoms in the contact. Usually, in most experiments, the bias voltage applied to the contact is 100 mV or lower. However, the hole peaks structure of the histogram can be kept unchanged up to 500 mV.

On the other hand, quantum effects are better appreciated on experiments in high vacuum at room temperature. Under these conditions, the contact choose its configuration by thermal diffusion of the atoms that rearrange on a time scale of milliseconds producing that the histogram peaks become more pronounced[51]. Conversely, thermal diffusion is slowed down at low temperatures, which limits the own structural exploration of the contact, but provide larger stability to the experimental setup and makes possible to stabilize single-atom contacts over long periods of time[52]. Despite the above, no qualitative changes in the histograms are observed, and the principal features are distinguishable independently of temperature[28].

The lifetime of the contact grows toward low stretching speeds. For stretching speeds higher than 1 nm/s, the lifetime is limited by the strain applied to the junction. Conversely, in the extremely slow limit, when the retraction speed is comparable to the surface diffusion velocity of gold atoms (0.02 - 0.003 nm/s at room temperature), the contact can entirely self-compensate for the induced strain leading to a more ordered structure[52–54]. Tsutsui et al. show that, on measurements performed at room temperature in vacuum and 100 mV bias, the single-atom contact lifetime changed from 0.02 to 200 s upon decreasing the stretching speed from 8 nm/s to 0.0008 nm/s. On the other hand, in the range from 30 to 4000 nm/s no influence was observed[47].

Atomic Chains

Some metals such as Au, Pt, and Ir can form long atomic chains before contact breaking due to the strong bonding of low-coordination atoms characteristic of 5d metals[55–57]. In 1998, using a MCBJ and an STM at liquid-helium temperatures, Yanson et al. found that the last conductance plateau at the value of ~ 1 G_0 can often persist despite an elongation much higher than the interatomic spacing, as the one shown in Figure 2.9. Imagine that a chain of atoms has formed before rupture, these atoms are then expected to return to the leads after the contact breaks. The distance to establish the contact again should be approximately equal to the length of the last plateau.

Further evidence comes from analyzing the distribution of lengths of the last conductance plateau on a histogram obtained during many cycles of contact breaking[58]. The distribution of plateau lengths in Figure 2.10 shows peaks equally separated by a distance that agrees with the expected bond distance in a chain of gold atoms (2.5 ± 0.2 Å). Therefore, each peak corresponds to atomic chains made out of different numbers of atoms. According to Figure 2.10, the most frequent contact length before rupture correspond to the size of two and one atoms. Sometimes plateaus till 2 nm in length are found and correspond to the formation of a chain with 7–8 atoms. Gold nanowires act as a one-dimensional conductor with a conductance very close to the quantum unit
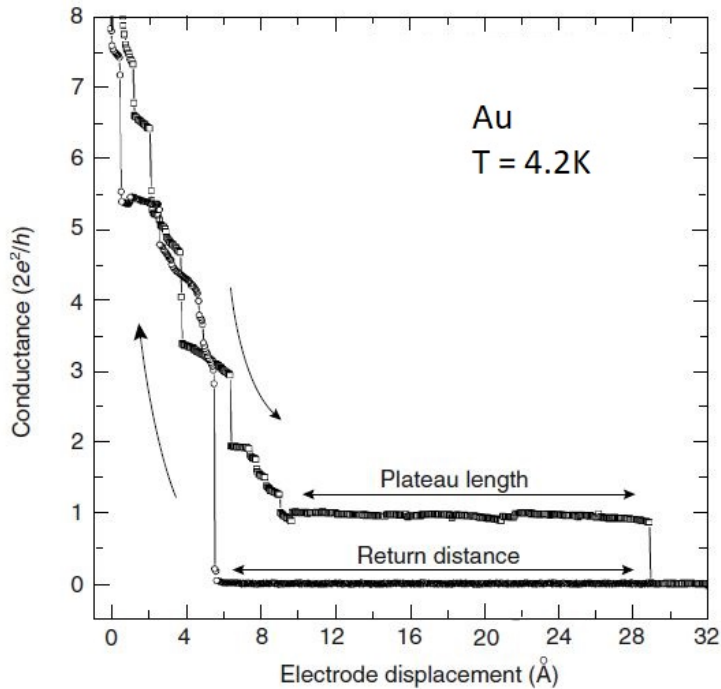
Figure 2.9: Conductance of gold as a function of the electrode displacement measured in MCBJ setup at 4.2 K. Adapted from[55].

G_0. Therefore, the main peak in the histogram around $1G_0$ (Figure 2.8), is due to the formation of single-atom contacts and also chains of atoms[59,60]. The formation of atomic chains is favored at low temperatures and they maximize its length (7-8 atoms) in the range from 150 to 200 K. At room temperature, atomic chains of about five atoms can form[61,62].

Conductance quantization involves a wide range of phenomenology. The series of peak values in the conductance histograms, or jumps in the conduction, differ from metal to metal. Histograms for sodium[13], potassium[63] and lithium[64] show peaks near 1, 3, 5, and 6 G_0 at low temperature. On the other hand, histograms of ferromagnetic materials show a single peak in the range of 1.5 to 3 G_0[65], which vanish at room temperature[46] and is modified in the presence of a magnetic field[66]. Aluminum is also a particular case. One-atom contacts of this metal consist of three partially transmitting quantum modes that conduct 1 G_0[67]. The histogram shows peaks near 1, 2, 3 and 4 G_0 similar to gold[68], which supports the fact that peaks represent preferential geometrical
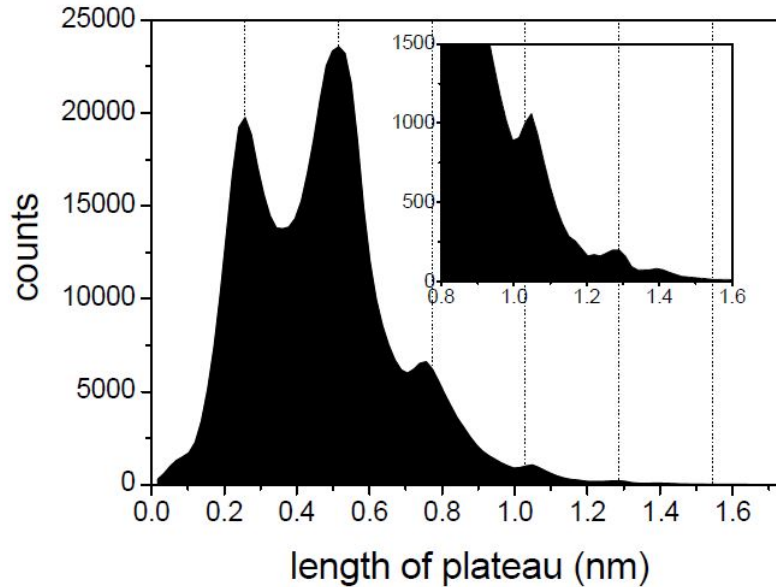
Figure 2.10: Distribution of lengths for the last conductance plateau of gold recorded with a MCBJ at 4.2 K in cryogenic vacuum. The plateau length is considered as the distance between the conduction points that fall in the range between 1.2 G_0 and 0.8 G_0. Retrieved and adapted from[1,58].

configurations of the contact, what is clearly shown in reference[69], where the authors construct atomic configuration histograms instead of conductance histograms. There is also a differentiation between regular conductance quantization that is defined by successive fill of single quantum modes and the moment when bulk crystalline order dominates electronic fluctuations and the contact formation mechanism changes. In that sense, Medina et al.[70] show evidence of ionic subshell, i.e., facet growing structures in nanocontacts of gold and aluminum at room temperature at the high conductance region ($G/G_0 > 15$) of histograms. The explanation for the previous facts will be no detailed here since this work is focused in conduction of atomic-sized contacts of gold that leads to regular quantization, but they are mentioned to recall the rich definition of conductance quantization.

Chapter 3

Design and principle of the MCBJ equipment

This section presents the design and operating principle of the MCBJ equipment built in the present work. The section describes the mechanical parts that constitute the equipment, the calculation of the attenuation factor that characterizes the design, explains the process for the sample preparation and shows the electronic circuit used to acquire the data.

As shown in the 3D schematics in Figure 3.1 and 3.2, the design of the MCBJ equipment consists of a three-point bending structure (shown at the right bottom) formed by two mobile metal rods placed 10 cm apart from each other, and a metal pushrod in between. The vertical position of the lateral supports is controlled by turning the central bold of the structure that holds them. The pushrod is fixed to an aluminum rail whose opposite end rests over a loudspeaker of 8 Ohms impedance and 8 inches of diameter (shown at the left bottom of Figure 3.1). The rail can pivot about a point 6.5 cm away from the pressure point of the pushrod over the sample substrate. The vibrations from the loudspeaker move the end of the rail upward and downward. Therefore, these vibrations are the ones that control the displacement of the pushrod vertically and, in consequence, the bending or relaxation of the steel substrate, or in other words, control the formation and breaking mechanism of the metallic contact.
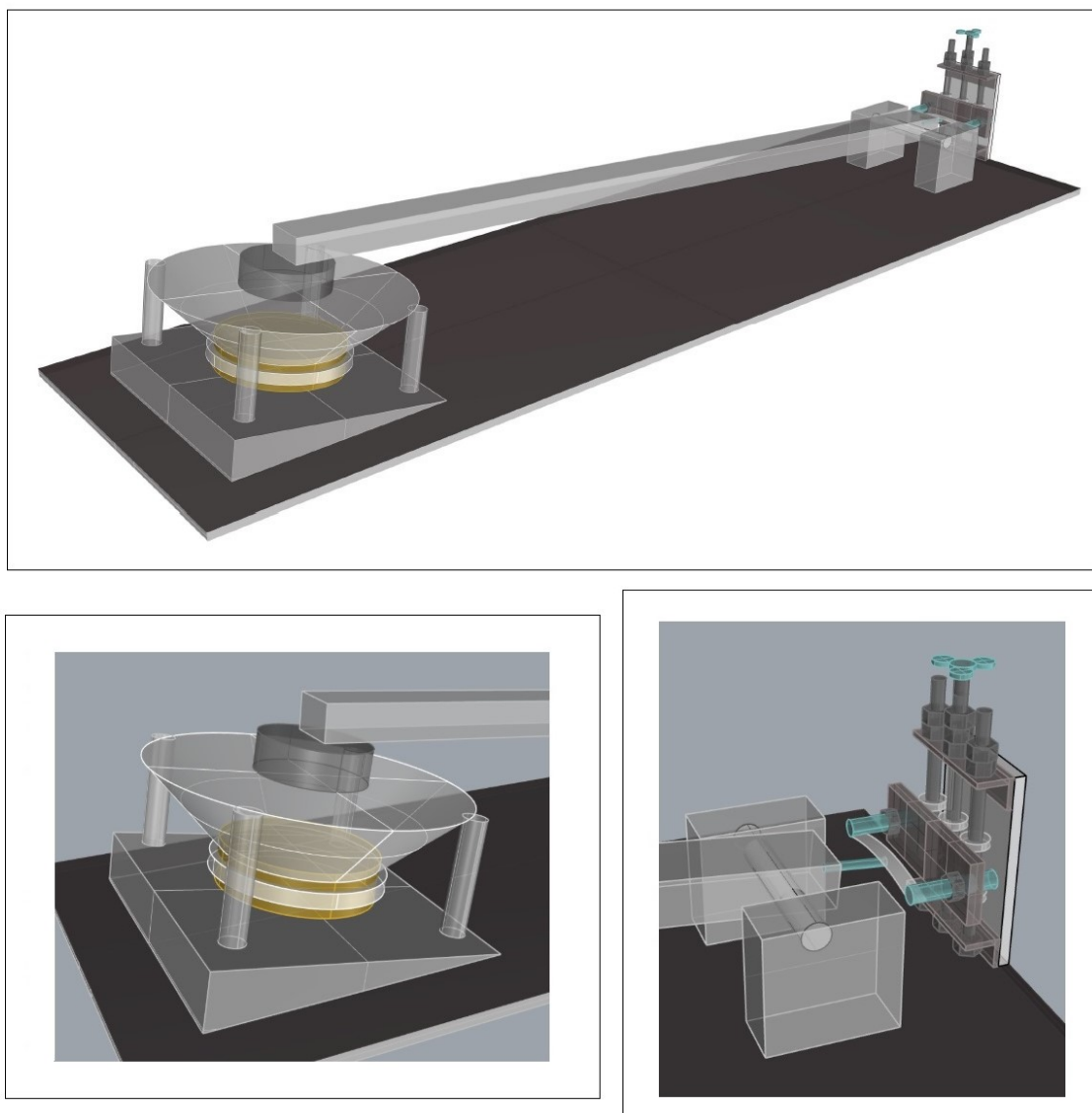
Figure 3.1: 3D schematics of the MCBJ equipment built in the research laboratory at Yachay Tech University.
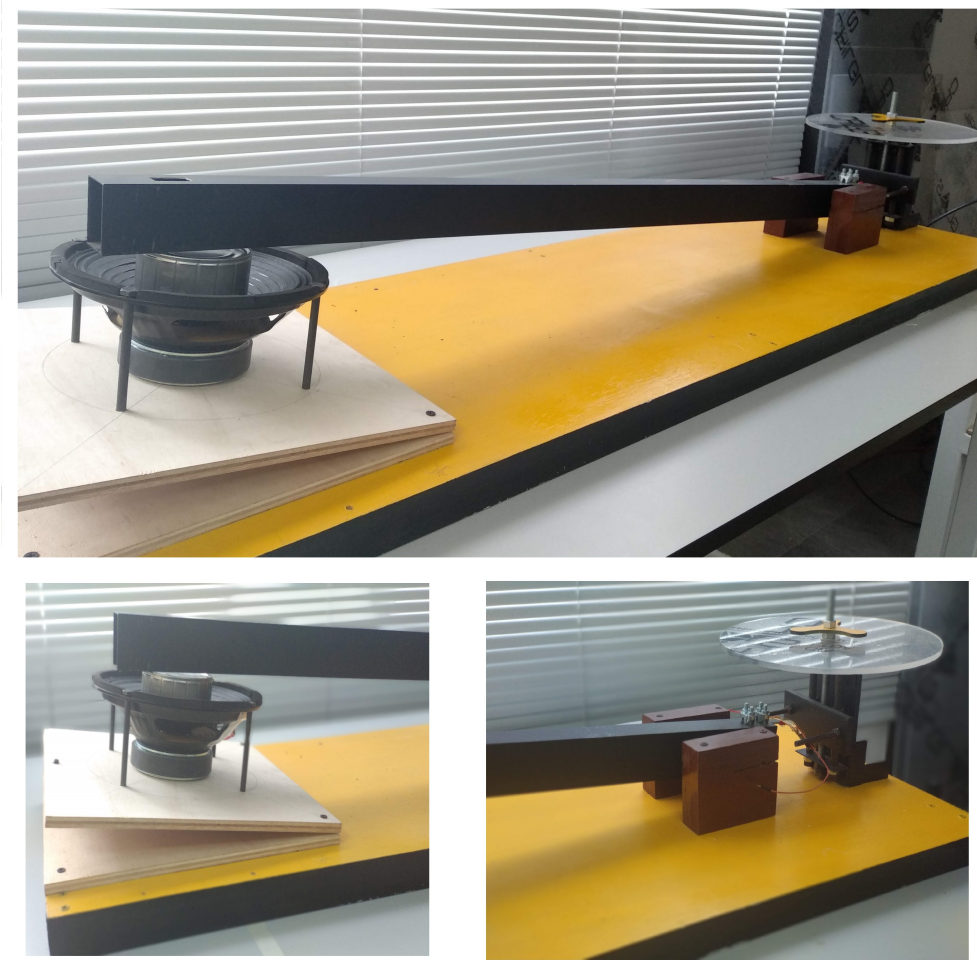
Figure 3.2: MCBJ equipment built in the research laboratory at Yachay Tech University.

The attenuation factor of the built MCBJ equipment can be estimated by the geometrical configuration of the system using the equation 2.17 from Chapter 2. The dimensions of the materials are $u = 0.1$ mm, $t = 4$ mm, and $L = 100$ mm for the size of the constriction in the wire, the thickness of the steel sheet, and the distance between the lateral supports, respectively. Using these values the attenuation factor is equal to:

$$r = \frac{\Delta x}{\Delta z} = \frac{6ut}{L^2} = 2.4x10^{-4}. \tag{3.1}$$

Considering the relation between the displacement z' of the rail end at the loudspeaker, which is $d' = 109$ cm away from the pivot point, and the displacement z of the rail end at the pushrod a distance $d = 6.5$ cm away from the pivot point:

$$\frac{z}{z'} = \frac{d}{d'}. \tag{3.2}$$

An amplitude displacement of $\Delta z' = 1$ mm at the loudspeaker moves the pushrod $\Delta z = 60\mu$m and consequently translates into an electrode separation of approximately $\Delta x = 14.4$ nm according to the attenuation factor.
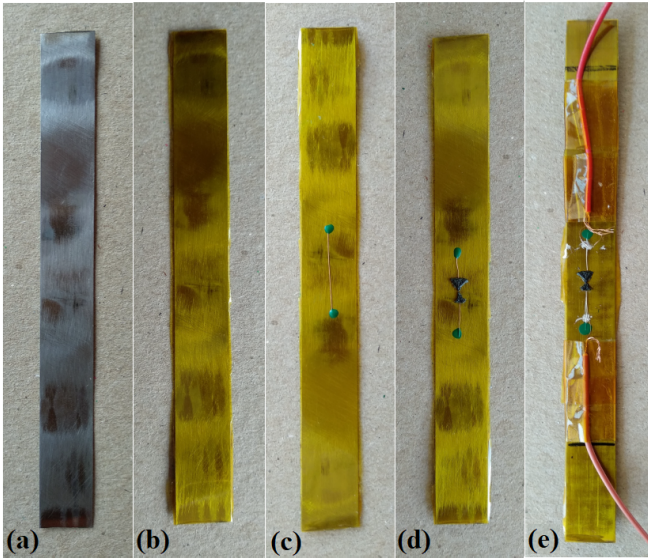
Figure 3.3: Top view of the sample preparation process. (a) Initial steel sheet substrate. (b) Steel sheet covered with insulating Kapton tape. (b) Neck-shaped gold wire fixed at the ends to the steel substrate with nail polish. (d) Two drops of epoxy adhesive applied one at each side of the constriction in the wire. (e) Copper wires welded to both ends of the gold wire using silver welding.

Figure 3.3 shows the steps needed in order to prepare the sample. First, a 10x1 cm spring steel substrate of 4mm thickness is covered with insulating Kapton tape (Figure 3.3 (a)-(b)). Second, a gold wire 2 cm long with a neck or constriction at the center is fixed to the steel substrate using nail polish (Figure 3.3 (c)). The constriction in the wire is previously cut, at approximately one-third of the wire width, by rolling the wire under a surgical knife using the handmade structure shown in Figure 3.4. Third, two triangular-shaped drops of epoxy adhesive are applied very close to the constriction without touching each other, leaving in between the neck of the wire (Figure 3.3 (d)). Figure 3.5 shows a close up view of wire neck between the facing epoxy drops. Finally, both ends of the gold wire are welded to copper wires using silver welding (Figure 3.3 (e)).

Figure 3.4: Guillotine used to cut the constriction on the gold wire. It consists of a fixed scalpel whose vertical position is adjusted using a micrometer screw. The gold wire is placed over a glass slide that can move following the ruler guides. In this way, the wire can roll under the scalpel and then it cuts a circular cross-section in the wire that forms the constriction.

Figure 3.5: Close up view of the constriction at the center of the wire used to form atomic-sized contacts.
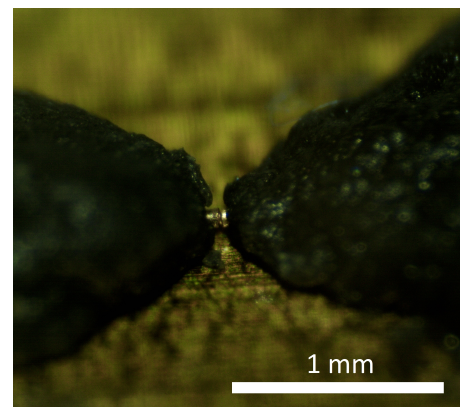
Figure 3.6 shows the overall circuit used for the operation of the equipment. A voltage divider with a variable resistor adjusts the bias voltage for the the gold wire. Then, the operational amplifier (op-amp) LM358P connected to a feedback resistor of $R_f = 100$ $K\Omega$ and a feedback capacitor of 22 pF amplifies the signal and converts the current to voltage. The output signal from the op-amp goes to the analog input of a National Instrument data acquisition DAQ device (NI USB-6210 16-bit), using a coaxial cable to reduce noise and interference from the environment. The wave generator based on the model XR2206 sends a sinusoidal signal to the audio amplifier TDA7293 that is connected to a 110V AC transformer to control the frequency and amplitude of the vibrations of the loudspeaker. To activate the trigger or acquisition of the data, a voltage comparison module compares the voltage from the sinusoidal wave sent to the audio amplifier, after passing through a voltage divider, with a reference value set by the voltage at the inverting input of the op-amp LM741CP. When the voltage coming from the sinusoidal wave is higher than the reference value, the output from the op-amp will be +Vcc; the DAQ board reads this value, and a LabVIEW program on the computer orders the DAQ to start acquiring the data. By modifying the reference voltage, the activation of the trigger is set close to the moment of rupture and formation of the atomic-sized contact. All the electric components are placed on the same breadboard and a simmetric power supply powers the circuit. A LabVIEW program on the computer shows the traces of voltage as a function of time and the progressive construction of the histogram during the experiment. It also saves the data to a text file for further analysis.
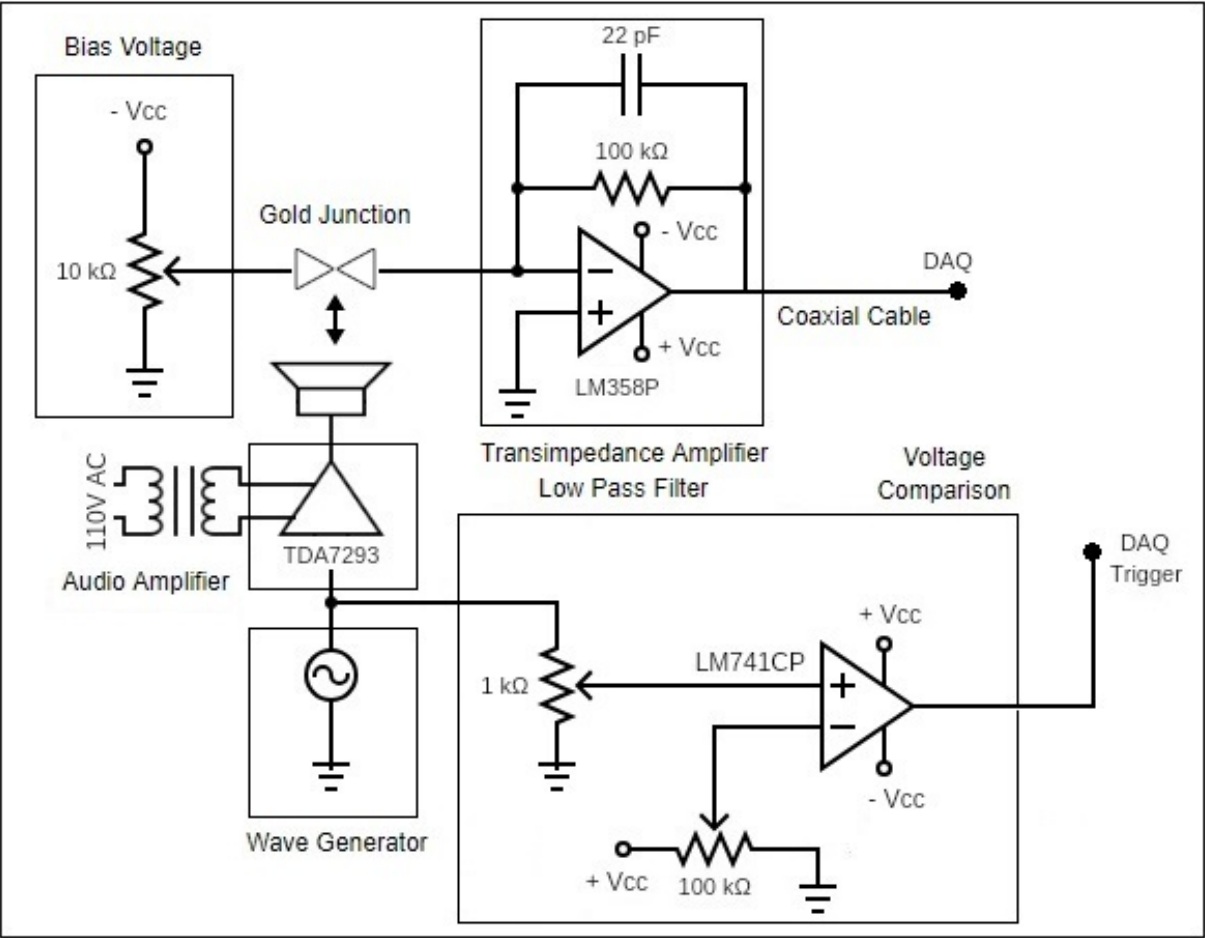
Figure 3.6: Circuit diagram that shows the electronic components and connections of the MCBJ equipment.

Chapter 4

Results & Discussion

This section presents experimental conductance measurements taken with the two techniques under consideration in this work to compare results. Technique A refers to the one that uses a Scanning Tunneling Microscope in the break junction regime (STM-BJ) built in the "Laboratorio de Bajas Temperaturas y Sistemas Nanométricos" at the University of Alicante in Spain. The technique B is the Mechanically Controllable Break Junction (MCBJ) setup built for this project in the physics research laboratory at Yachay Tech University. All the experiments are carried out in air and room temperature conditions.

4.1   Description of the experimental conditions

4.1.1   Technique A

Figure 4.1 shows on the left the microscope used to take the measurements. It employs two gold sheets as electrodes to form the contact. The sheets of 1.0 x 1.3 cm long and $100\,\mu$m of thickness fit on support structures, as shown in Figure 4.1 to the right. These supports are twisted with respect to each other and fixed, one to a mobile part in the head of the microscope and the other one to the base. The mobile part of the microscope, at which is fixed one of the electrodes, rests on four piezo piles, which allow it to move perpendicular to the base of the microscope. The procedure of how to create the piezo piles and how they work is detailed in reference[71]. The metallic contact is

established at the point where the two gold sheets meet. By applying ramps of high voltage to the piezo piles, the gold sheet electrodes are approached or separated at a velocity of approximately 300 nm/s, and the contact can be formed and broken repeatedly.
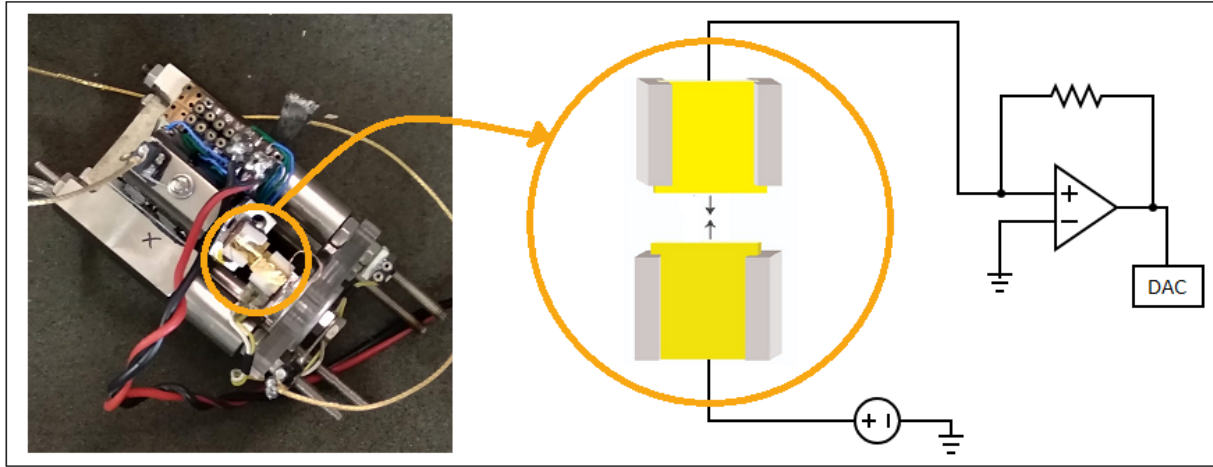
Figure 4.1: STM microscope in the break junction regime used to measure conductance through atomic-sized contacts built in the LT-Nanolab of the University of Alicante (left). Representation of the circuit and type of electrodes used to form the contact (right).

The electrode at the base of the microscope connects to a bias voltage. The current that flows through the other electrode is measured using a DLPCA-200 femto I/V converter with trans-impedance gain of 10^5 V/A, 400 kHz of upper cut-off frequency, and a maximum input current or maximum output voltage of 0.1 mA or 10 V respectively. The I/V converter is then connected to a Digital Analogical Converter (DAC), and a LabVIEW program on the computer shows and records the signal in the form of conductance versus voltage ramp applied to the piezo piles. During the experiment, the microscope is placed inside an aluminum box with BNC (Bayonet Neill-Concelman) external connectors to the IV converter and bias voltage, and coaxial cables for the wiring inside the box apart from the leads near the gold wires. Thus, the lowest voltage level signal oscillations remains below 0.01 V.

The STM-BJ setup has a sampling rate of 10 traces per second and 10-bit resolution (1024 points) in a time window of 100 ms. Figure 4.2 shows examples of traces of conductance taken with the STM-BJ for the process of breaking (a) and formation (b) of the contact. The maximum conductance is 14 G_0, which results from the maximum output voltage of the IV converter and the applied bias voltage which is set to 97 mV. The inset shows the full voltage ramp range. It goes from 0.0 to 0.5 V. However, since the gold sheet electrodes are not totally fixed to their supports, they move slightly during the experiment, changing the point of contact. Therefore, it will be necessary to vary the amplitude of the voltage ramp at the piezo piles avoiding loosing the signal.
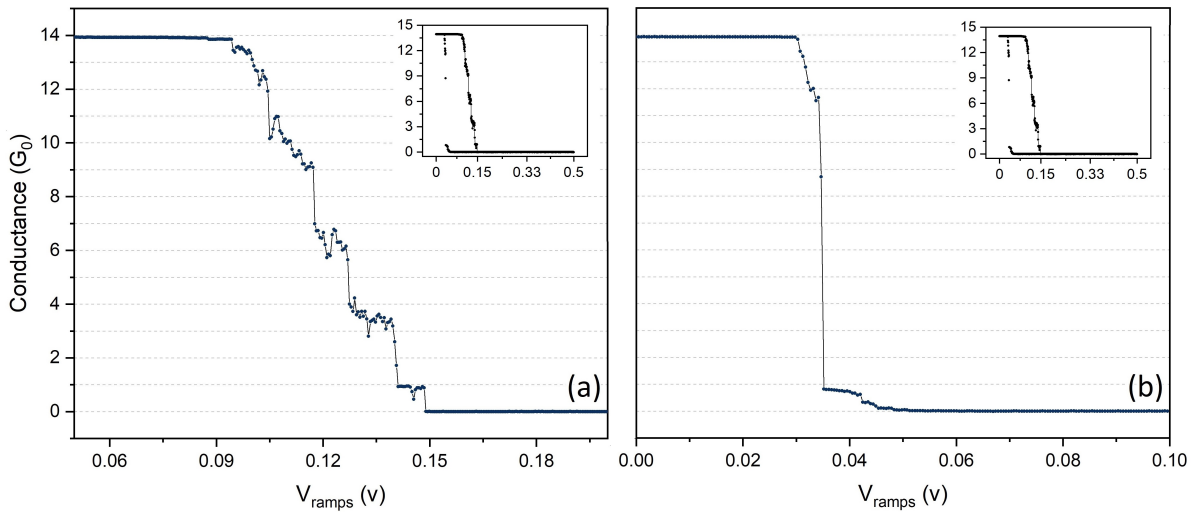
Figure 4.2: Typical conductance traces in units of the quantum of conductance as a function of the ramp voltage applied to the piezo piles of the STM during the process of breaking (a) and formation (b) of the contact.

Figure 4.2 (a) clearly shows how the conductance decreases in a step-wise manner as the gold sheet electrodes get apart. The plateaus have a negative slope for high values of the conductance and become nearly flat for the lowest one, near integer values, such as the plateau at 1 G_0 in the

graph. After rupture, the atoms rearrange at the surface, and the conductance drops to zero. In Figure 4.2 (b), from right to left, an exponential increase of the conductance is observed as the gold sheets approximate when the ramp voltage reverses from 0.5 to 0.0 V. After this, the contact is established with a jump to a conductance near to 1 G_0 and grows abruptly to higher values that depend on the arrangement of the atoms at the electrodes surface.

4.1.2   Technique B

The curves of time evolution of conductance obtained with the MCBJ have a time window of 250 ms and 10000 data points. The rate sampling is approximately 4 curves per second and depends on the trigger activation. Each shot of the trigger captures, on average, two continuous traces, one of formation and one of rupture. The frequency of repetition of these events varies and is not always synchronized with the trigger. Then, sometimes no traces are captured at all. However, this does not affect the sampling significantly, and it is possible to have thousands of conductance traces in less than 15 minutes. Additionally, during the experiment, it is necessary to adjust the position of the lateral supports of the three-point bending structure when required in order not to lose the signal since the repetition frequency of rupture and formation events also changes or is lost as the experiment runs.

The lowest voltage level signal oscillates between -0.1 V and 0.1 V and sometimes these noise oscillations are higher. A high voltage supply increases the noise level and also increments variations of conductance values out of the flat range within the plateaus. The bias voltage and power supply for the measurements was set to V_{bias} = 220 mV and V_{supply} = 6 V, respectively, in such a way that the output voltage corresponding to a conductance of 1 G_0 would be 1.70 V, relatively far from the noise range, and resulting in a maximum conductance value of 2.75 G_0.

Due to the implemented triggering system, it is necessary to use the lowest frequency allowed by the wave generator (see Figure 3.6), that corresponds to 0.72 Hz, in order to increase, up to the

highest possible, the time at which the events of interest (formation and rupture) take place. In other words, the objective is to reach the slowest posible stretching speed. However, at this frequency, the wave signal saturates and produces vibrations of different amplitudes at the loudspeaker, which results in the formation of incomplete traces, as can be seen in Figure 4.3 (a). Thus, for the statistical analysis, only traces that complete a formation and break cycle, passing through all values between 0 and 2.75, are taken into account. An example of this consideration is represented in Figure 4.3. Because of the nature of the noise observed in the graphs, the main sources of instability in the setup are the unstable amplitude vibrations of the loudspeaker and the noise produced by the voltage supply at the breadboard where all the electric components are connected.

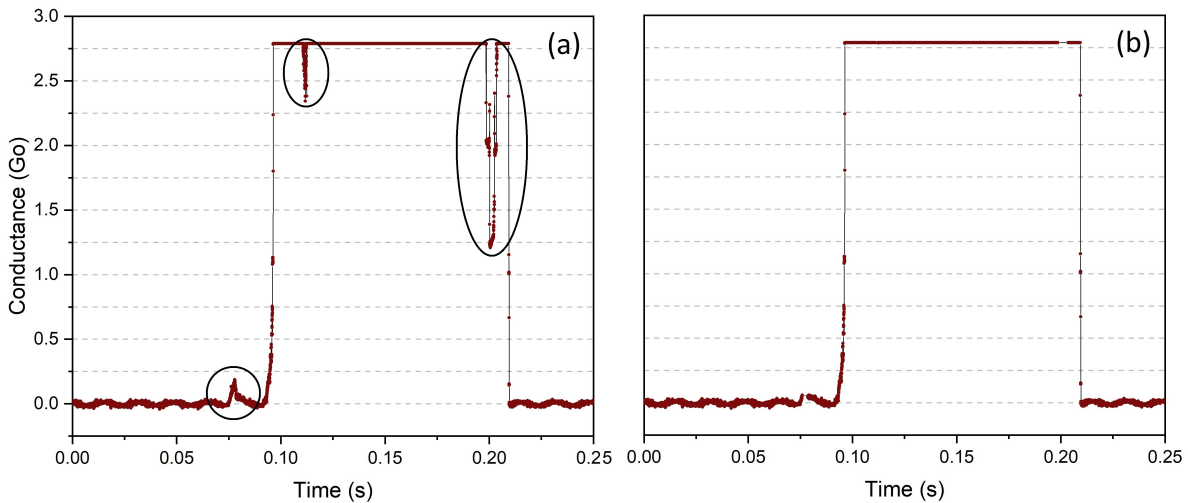Figure 4.3: Example of the time evolution of the conductance during the breaking and rupture of the contact using the MCBJ equipment. Traces from incomplete cycles of rupture and formation of the contact form during the experiment (marked with circles in panel (a)), and are not considered for the statistical analysis. (b) Conductance curve that includes only complete cycles of formation and rupture.

4.2 Histograms of conductance

4.2.1 Technique A

Figures 4.4 and 4.5 shows histograms accumulated from consecutive rupture and formation traces in panel (a), and just from rupture events in panel (b). The sample used for the measurements shown in the first figure was cleaned in a piranha solution[72] (hydrogen peroxide and sulfuric acid 1:3) before the experiment, as opposed to the sample for the set of measurements of Figure 4.5, which remained in the non-sterile environment of the laboratory and no cleaning process was done before the measurement. Figure 4.4 shows the typical histogram for gold reported in the literature. It clearly shows up to five peaks. Based on Gaussian fits (not shown in the Figure), their positions are $0.921 \pm 0.004\ G_0$, $1.771 \pm 0.025\ G_0$, $2.682 \pm 0.030\ G_0$, $3.377 \pm 0.06\ G_0$ and $4.269 \pm 0.06\ G_0$. The counts from the contribution of tunneling observed during formation traces are below the peak at $1\ G_0$ in Figures 4.4 (a) and Figure 4.5 (a). Figure 4.5 differs from the typical histogram of gold due to the backscattering effects of adsorbates from atmospheric contamination. These changes are better visualized in Figure 4.6. The main feature is the formation of a peak around 0.2 pointed out in Figure 4.6 (b). Additionally, all the peaks are broader, the count for non-integer values increases in the entire conductance range (δ), and the height of the peaks near $2\ G_0$ and $3\ G_0$ grows.

Figure 4.4: Conductance histograms for gold nanowires at room temperature in air measured with the STM-BJ approach and 97 mV bias. (a) Histogram built with 5290 consecutive formation and breaking curves. (b) Histogram based on 2645 consecutive breaking curves. The gold samples were cleaned in a piranha solution previous to the experiment. Notice that up to five peaks are resolved.

Figure 4.5: Conductance histograms for gold nanowires at room temperature in air measured with the STM-BJ approach and 97 mV bias. (a) Histogram built with 1979 consecutive formation and breaking curves. (b) Histogram based on 1010 consecutive breaking curves. The typical features of the histograms change due to the presence of adsorbates from atmospheric contamination (see text).

Figure 4.6: Effects of the presence of adsorbates from atmospheric contamination in the conductance histogram of gold nanowires. Histograms from Figures 4.5 (gray) and 4.4 (blue) normalized to the maximum count of the peak at 1 G_0. The arrows indicate the main differences (see text).

4.2.2 Technique B

The gold wire sample used to take the measurements with the MCBJ equipment described in Chapter 3, has been prepared and mounted as indicated in Figure 3.3. It has been exposed to the laboratory environment during a couple of months before the measurement, and no cleaning process was implemented.

A set of example traces are shown in Figure 4.7. The curve (a) shows how the conductance decreases in three steps as the electrodes move apart with a well defined plateau at 1 G_0. Conversely, curve (b) shows two decreasing steps, and in curve (c) a long plateau below 0.5 G_0 appears due to the presence of adsorbates from atmospheric contamination. Curve (d) illustrates the process of contact formation. As the electrodes get closer the conductance increases exponentially and suddenly jumps to contact near 1 G_0, after which reaches the maximum conductance.

Figure 4.8 shows the histograms accumulated from complete rupture and formation events (a), and just from complete rupture traces (b), captured with the triggering system of the MCBJ equipment. Three main peaks are resolved whose positions are 0.981 ± 0.005 G_0, 1.825 ± 0.012 G_0, 2.566 ± 0.022 G_0 (based on a Gaussian fit not shown in the Figure) and correspond to the conductance quantization in gold nanowires. The count from the contribution of tunneling observed in contact formation events falls below the peak at 1 G_0 shown Figure 4.8 (b). The features of the histogram are similar to those shown in Figure 4.5. The peaks are broader, the count for non-integer values increases and a peak below 0.5 G_0 forms, positioned at 0.306 ± 0.027 G_0, which suggests the presence of adsorbates from atmospheric contamination. This comparison is represented in Figure 4.9. Also, note that the quality of the measurements with both techniques is similar. Finally, Figure 4.10 compares the histograms obtained with the MCBJ, and the histograms that characterize a clean gold wire in the range from 0 G_0 and 2.75 G_0 obtained with the STM-BJ. The same variations observed in Figure 4.6 can be appreciated.
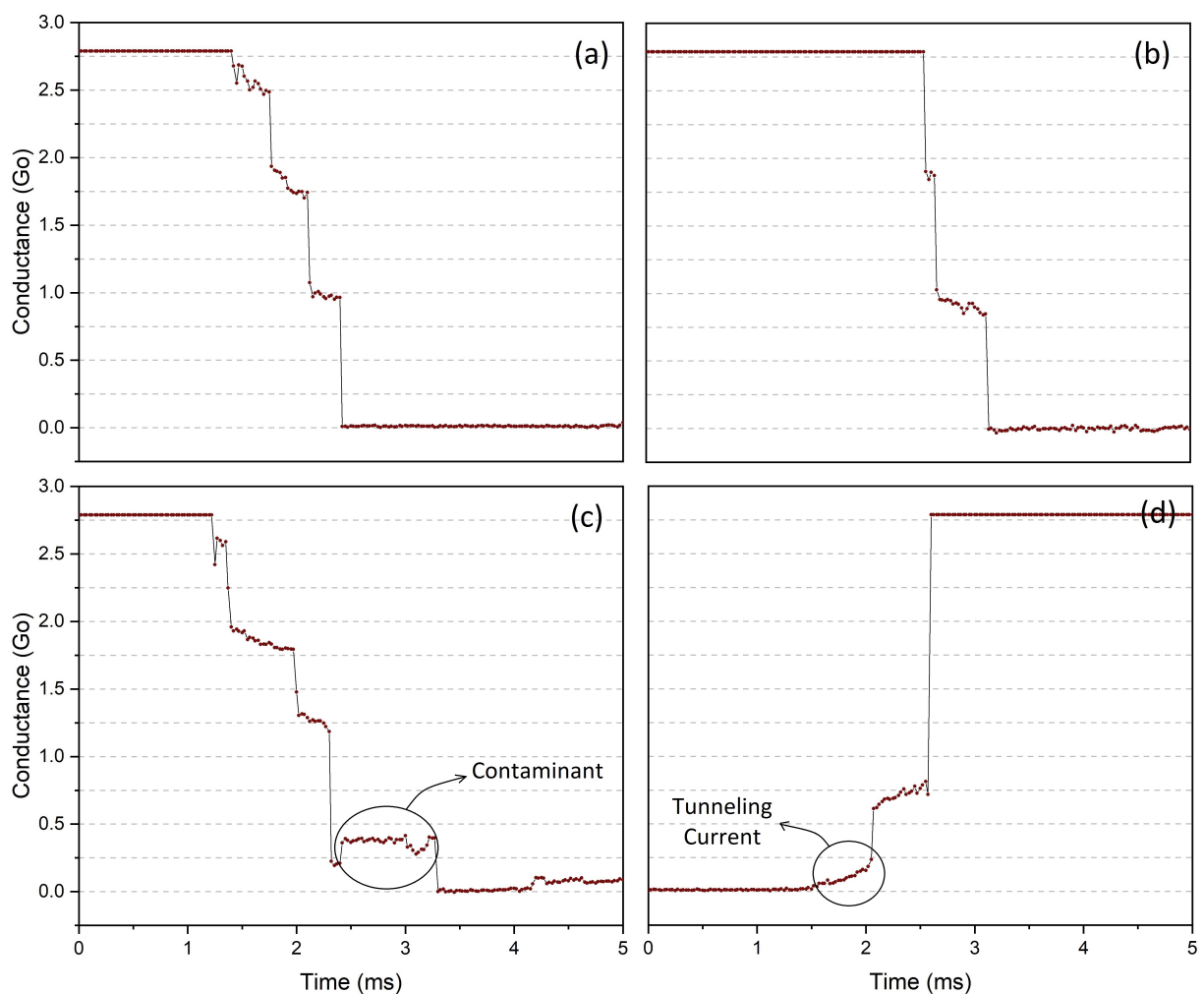
Figure 4.7: Set of four traces of rupture (a) - (c) and formation (d) of an atomic-sized contact of gold which clearly show quantized conductance steps. The measurements were obtained with the MCBJ equipment at room temperature in air applying a bias voltage of 220 mV.
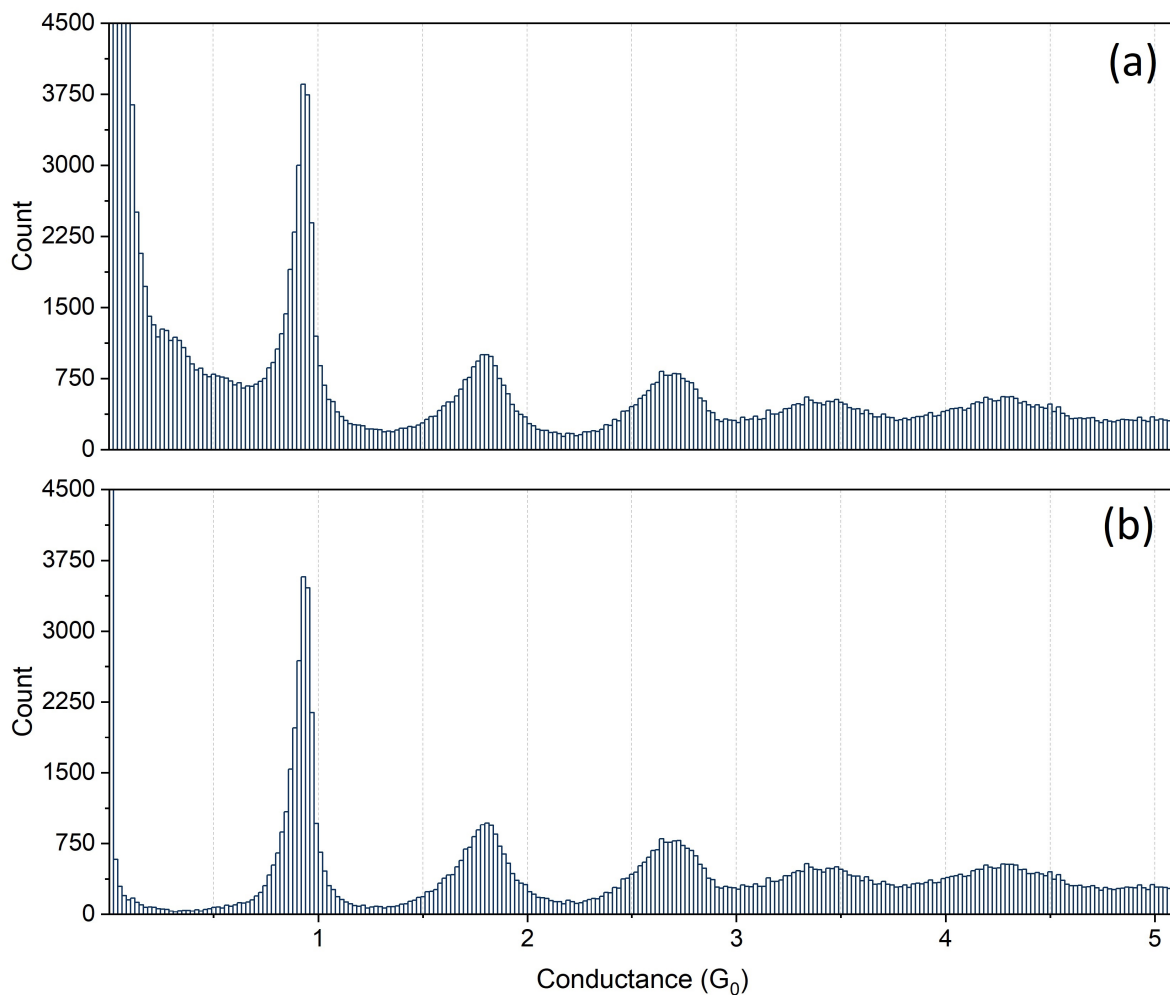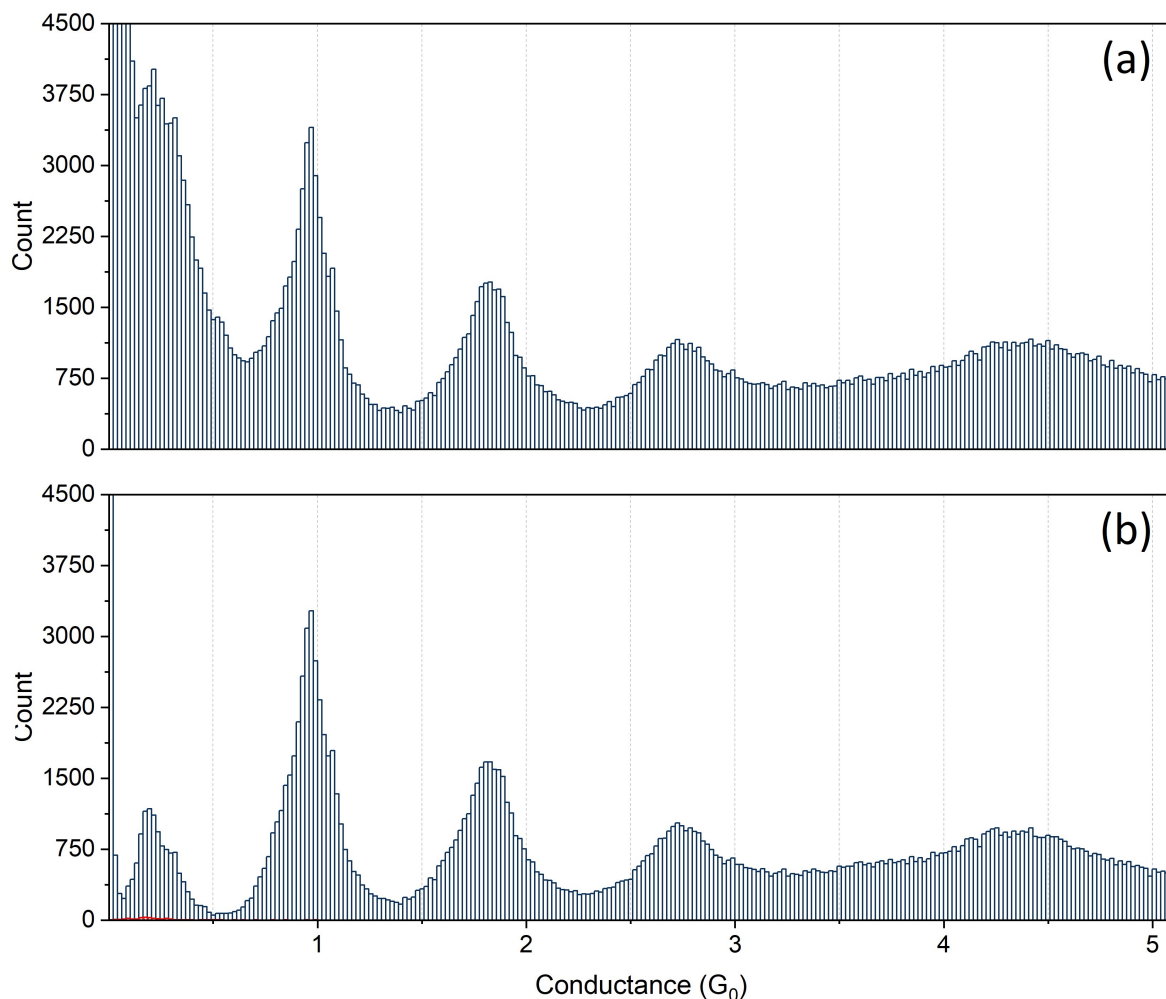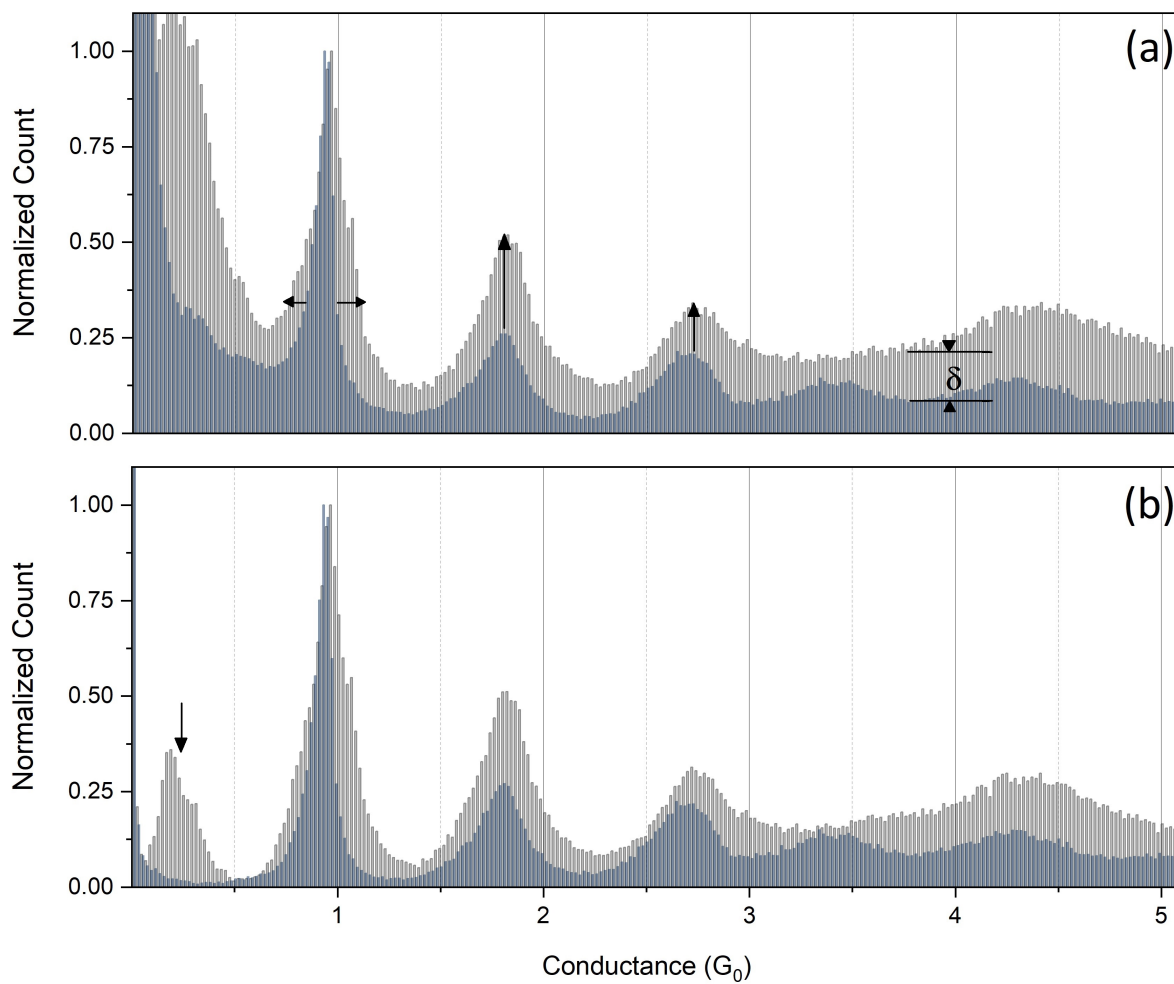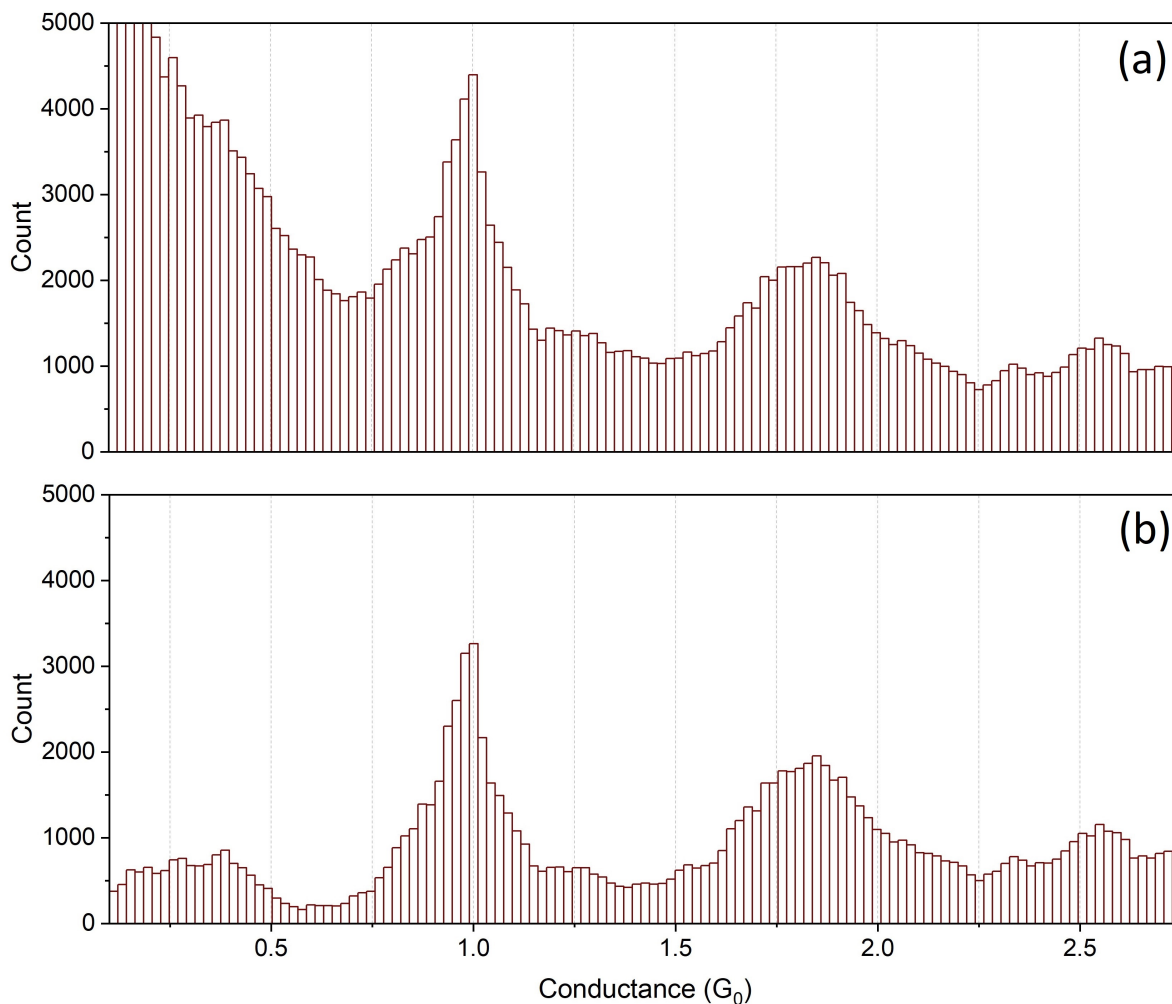
Figure 4.8: Conductance histograms for gold nanowires at room temperature in air measured with the MCBJ approach and 220 mV bias. (a) Histogram built with conductance curves captured after 5349 trigger activation times, considering rupture and formation events. (b) Histogram built with conductance curves of rupture events captured after 1188 trigger activation times. Notice that up to three peaks are resolved and the histograms features suggest the presence of adsorbates from atmospheric contamination.
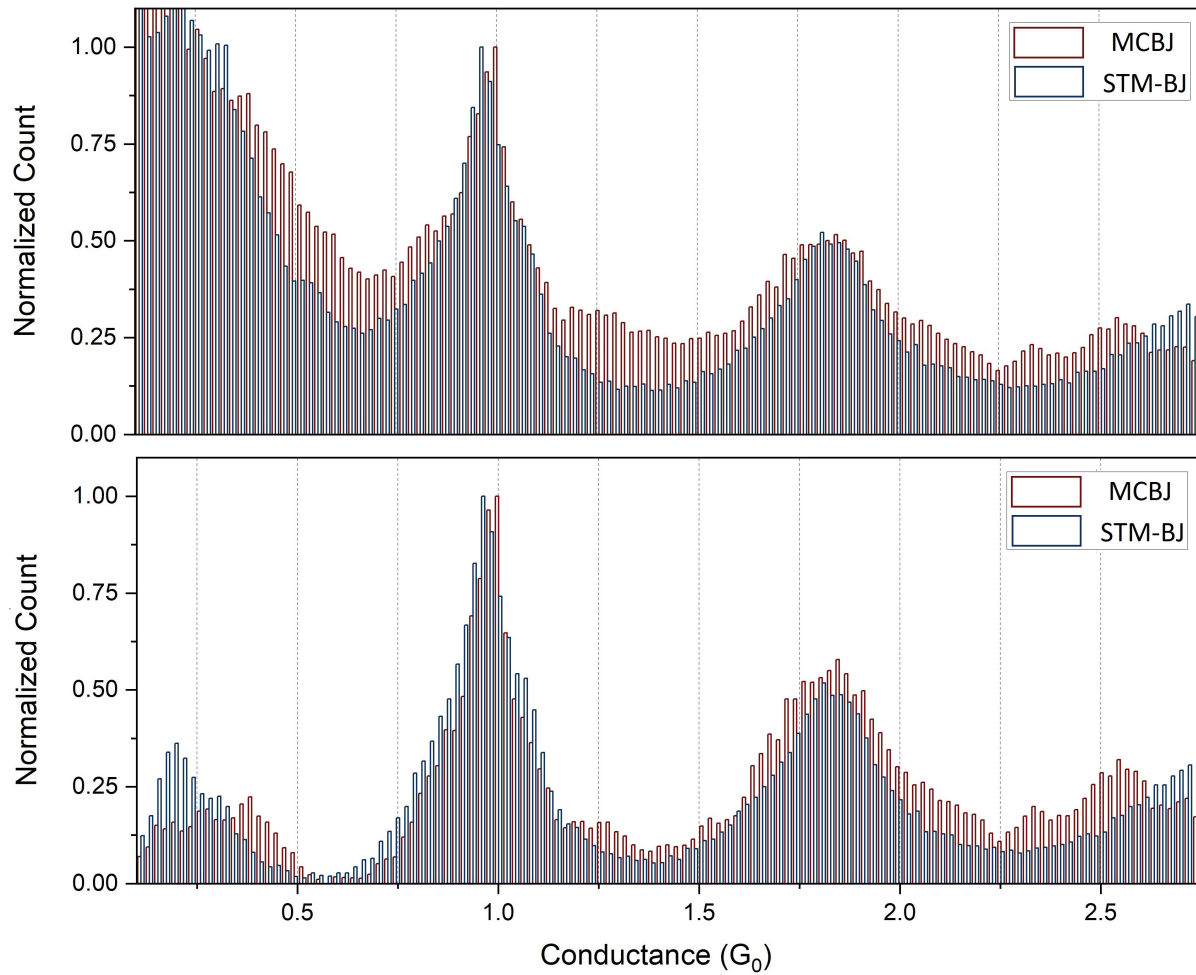
Figure 4.9: Comparison of the measurements performed with the MCBJ (red) and STM-BJ (blue) setups. The histograms from Figures 4.8 (red) and 4.5 (blue), normalized to the maximum count of the peak at 1 G_0, are shown.
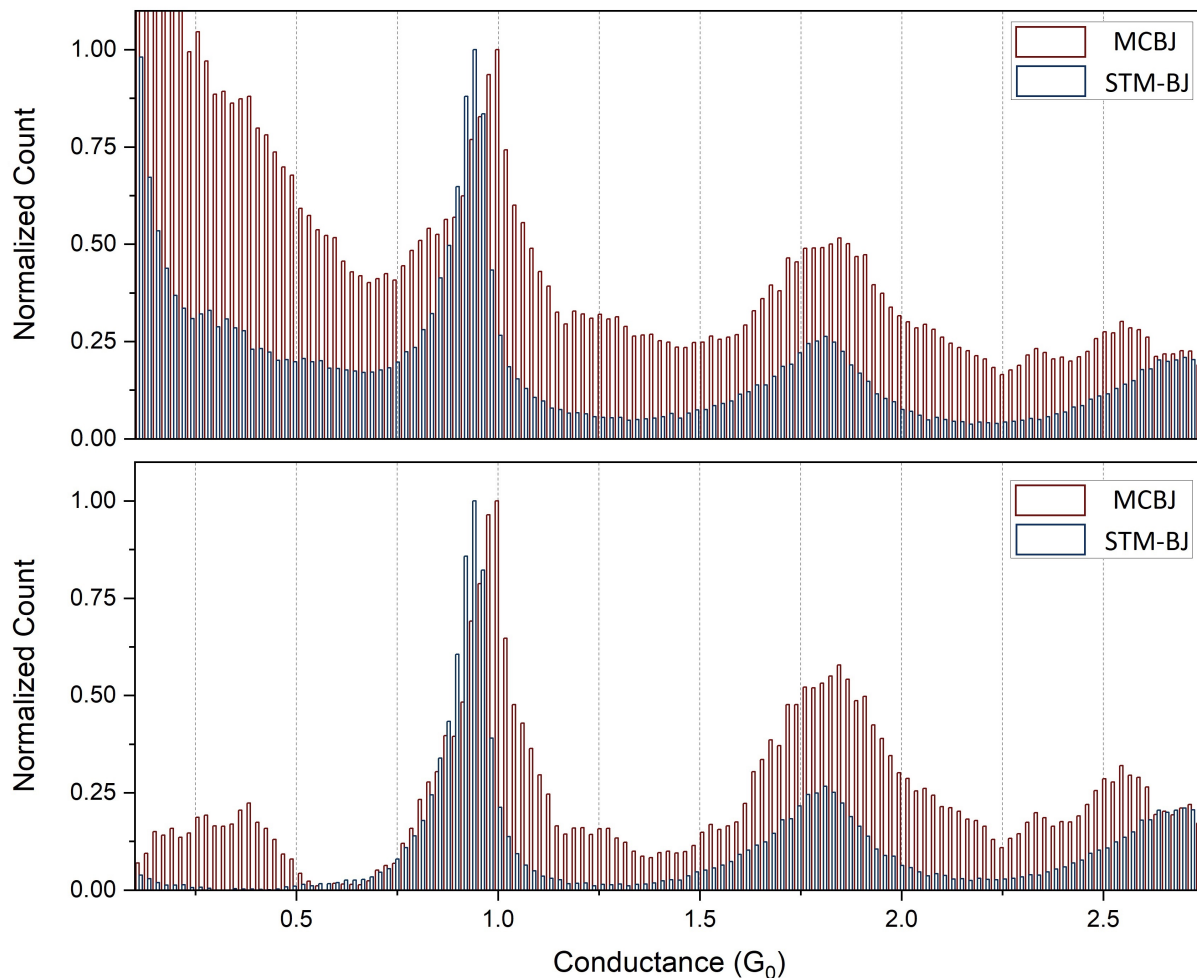
Figure 4.10: Comparison of the measurements performed with the MCBJ (red) and STM-BJ (blue)
setups. The histograms from Figures 4.8 (red) and and 4.4 (blue), normalized to the maximum
count of the peak at 1 G_0, are shown. Backscattering effects due to the presence of adsorbates
from atmospheric contamination ca be appreciated in the histogram of the MCBJ equipment (red).
These are the formation of a peak below 0.5 G_0 shown at the bottom, the broadening of the peaks,
the increase of the counts at non integer values and a higher peak at 2 G_0.

Chapter 5

Conclusions & Recommendations

The Mechanically controllable break junction (MCBJ) experimental setup is one of the main techniques employed in the study of electronic transport properties at the nano-scale. This work has described the construction of an innovative, robust, low-cost, and simple equipment to measure conductance through atomic-sized contacts of gold and obtain statistical information of the experimental data. The graphs from Chapter 4 shows that the proposed MCBJ setup has a resolution comparable to that of research equipment, such as the STM-BJ built in the LT-Nanolab of the University of Alicante, although the maximum conductance range is limited. The built MCBJ equipment introduces a technique to form atomic-sized contacts never used before. It has the advantage that replaces the use of piezoelectric materials that are part of conventional types of MCBJ, with the action of the vibrations of a loudspeaker, which reduces the cost of fabrication significantly, therefore being more accessible to incorporate into undergraduate advanced physics programs.

There are other experimental realizations to form atomic-sized contacts which also do not use piezoelectric materials. Such approaches display quantized conductance steps, for example, by simply tapping on a table with two attached gold wires[24,73] or using electromagnetic relays[23,46]. However, the presented MCBJ setup offers finer control over the process of separating and re-connecting the gold electrodes in comparison with the latter techniques. Also, other setups with similar pedagogical purposes have been built. For instance, Huismann et al.[74] present an apparatus available in a public space where a general audience can manually thin a gold wire and monitor

its conductance in real-time. However, this setup employs advanced lithography to fabricate the break junctions. In contrast, the preparation and assembly of the sample for the MCBJ described here is simple and can be done by any student or professional, not requiring experience or specific skills in advanced techniques such as lithography. On the other hand, the setup of reference [18] uses a micrometer to bend the substrate where the gold wire is attached. Nevertheless, the latter equipment, like the one described by Huismann et. al, does not include an automatic mechanism that allows repeating cycles of rupture and formation continuously. The MCBJ of this work does.

Further implementations to improve the data acquisition and definition of the results can be realized. For example, starting by replacing the wave generator that defines the amplitude and frequency of the vibrations at the loudspeaker, with one that works better in the range of sub-hertz. Also, to minimize the noise by building the circuit in a metal box with BNC connectors and using coaxial cables for most of the wiring. In this way, it will be possible to increase the maximum output voltage from the op-amp without disturbing the signal and thereby, to expand the conductance range. Finally, consider the fact the National Instruments data acquisition (DAQ) unit, described as part of the MCBJ setup, is not essential to carry out the experiment. It can be replaced with an inexpensive storage oscilloscope and obtain similar results.

Bibliography

[1] Agraıt, N.; Yeyati, A. L.; Van Ruitenbeek, J. M. Quantum properties of atomic-sized conduc-
tors. *Physics Reports* **2003**, *377*, 81–279.

[2] Wang, J.; Guo, H.; Mozos, J.-L.; Wan, C.; Taraschi, G.; Zheng, Q. Capacitance of atomic
junctions. *Physical Review Letters* **1998**, *80*, 4277.

[3] Terabe, K.; Hasegawa, T.; Nakayama, T.; Aono, M. Quantized conductance atomic switch.
Nature **2005**, *433*, 47–50.

[4] Zhou, X.-S.; Liang, J.-H.; Chen, Z.-B.; Mao, B.-W. An electrochemical jump-to-contact
STM-break junction approach to construct single molecular junctions with different metallic
electrodes. *Electrochemistry Communications* **2011**, *13*, 407–410.

[5] Xu, B.; Tao, N. J. Measurement of single-molecule resistance by repeated formation of
molecular junctions. *Science* **2003**, *301*, 1221–1223.

[6] Li, C.; He, H.; Bogozi, A.; Bunch, J.; Tao, N. Molecular detection based on conductance
quantization of nanowires. *Applied Physics Letters* **2000**, *76*, 1333–1335.

[7] Gimzewski, J.; Möller, R. Transition from the tunneling regime to point contact studied using
scanning tunneling microscopy. *Physical Review B* **1987**, *36*, 1284.

[8] Muller, C.; Van Ruitenbeek, J.; De Jongh, L. Experimental observation of the transition from weak link to tunnel junction. *Physica C: Superconductivity* **1992**, *191*, 485–504.

[9] Sabater Piqueres, C. Theoretical and experimental study of electronic transport and structure in atomic-sized contacts. Ph.D. thesis, **2013**.

[10] Zhou, C.; Muller, C.; Deshpande, M.; Sleight, J.; Reed, M. Microfabrication of a mechanically controllable break junction in silicon. *Applied Physics Letters* **1995**, *67*, 1160–1162.

[11] Agrait, N.; Rodrigo, J.; Vieira, S. Conductance steps and quantization in atomic-size contacts. *Physical Review B* **1993**, *47*, 12345.

[12] Olesen, L.; Laegsgaard, E.; Stensgaard, I.; Besenbacher, F.; Schio/tz, J.; Stoltze, P.; Jacobsen, K.; No/rskov, J. Quantized conductance in an atom-sized point contact. *Physical Review Letters* **1994**, *72*, 2251–2254.

[13] Krans, J.; Van Ruitenbeek, J.; Fisun, V.; Yanson, I.; De Jongh, L.; J, The signature of conductance quantization in metallic point contacts. *Nature* **1995**, *375*, 767.

[14] Pascual, J.; Mendez, J.; Gomez-Herrero, J.; Baro, A.; Garcia, N.; Landman, U.; Luedtke, W.; Bogachek, E.; Cheng, H.-P. Properties of metallic nanowires: from conductance quantization to localization. *Science* **1995**, *267*, 1793–1795.

[15] Gai, Z.; He, Y.; Yu, H.; Yang, W. Observation of conductance quantization of ballistic metallic point contacts at room temperature. *Physical Review B* **1996**, *53*, 1042.

[16] Nazarov, Y. Quantum transport : introduction to nanoscience; *Cambridge University Press*, **2009**.

[17] Nitzan, A. Electron transmission through molecules and molecular interfaces. *Annual Review of Physical Chemistry* **2001**, *52*, 681–750.

[18] Tolley, R.; Silvidi, A.; Little, C.; Eid, K. Conductance quantization: A laboratory experiment in a senior-level nanoscale science and technology course. *American Journal of Physics* **2013**, *81*, 14–19.

[19] Maxwell, J. A treatise on electricity and magnetism; Dover Publications: New York, **1954**.

[20] Sharvin, Y. V. A possible method for studying fermi surfaces. *Journal of Experimental and Theoretical Physics* **1965**, *21*, 655.

[21] Landauer, R. Spatial variation of currents and fields due to localized scatterers in metallic conduction. *IBM Journal of Research and Development* **1957**, *1*, 223–231.

[22] Ihn, T. Semiconductor nanostructures : quantum states and electronic transport; *Oxford University Press*: Oxford New York, **2010**.

[23] Ott, F.; Lunney, J. Quantum conduction: a step-by-step guide. *Europhysics news* **1998**, *29*, 13–16.

[24] Costa-Krämer, J.; Garcia, N.; Garcia-Mochales, P.; Serena, P. Nanowire formation in macroscopic metallic contacts: quantum mechanical conductance tapping a table top. *Surface Science* **1995**, *342*, L1144–L1149.

[25] Yasuda, H.; Sakai, A. Conductance of atomic-scale gold contacts under high-bias voltages. *Physical Review B* **1997**, *56*, 1069.

[26] Pace, C.; Giusi, G.; Crupi, F.; Lombardo, S. A. Detection and classification of single-electron jumps in Si nanocrystal memories. *IEEE Transactions on Instrumentation and Measurement* **2008**, *57*, 364–368.

[27] Evers, F.; Korytár, R.; Tewari, S.; van Ruitenbeek, J. M. Advances and challenges in single-molecule electron transport. *arXiv e-prints* **2019**, arXiv:1906.10449.

[28] Sirvent, C.; Rodrigo, J.; Agrait, N.; Vieira, S. STM study of the atomic contact between metallic electrodes. *Physica B: Condensed Matter* **1996**, *218*, 238–241.

[29] Brandbyge, M.; Schio/tz, J.; So/rensen, M.; Stoltze, P.; Jacobsen, K.; No/rskov, J.; Olesen, L.; Lægsgaard, E.; Stensgaard, I.; Besenbacher, F. Quantized conductance in atom-sized wires between two metals. *Physical Review B* **1995**, *52*, 8499.

[30] Landman, U.; Luedtke, W.; Salisbury, B. E.; Whetten, R. L. Reversible manipulations of room temperature mechanical and quantum transport properties in nanowire junctions. *Physical Review Letters* **1996**, *77*, 1362.

[31] Xiang, D. Fabrication and utilization of mechanically controllable break junction for bioelectronics; *Forschungszentrum Jülich GmbH*, **2012**.

[32] Yi, Z.; Banzet, M.; Offenhäusser, A.; Mayer, D. Fabrication of nanogaps with modified morphology by potential-controlled gold deposition. *Rapid Research Letters* **2010**, *4*, 73–75.

[33] Schirm, C.; Matt, M.; Pauly, F.; Cuevas, J. C.; Nielaba, P.; Scheer, E. A current-driven single-atom memory. *Nature Nanotechnology* **2013**, *8*, 645.

[34] Sydoruk, V.; Xiang, D.; Vitusevich, S.; Petrychuk, M.; Vladyka, A.; Zhang, Y.; Offenhäusser, A.; Kochelap, V.; Belyaev, A.; Mayer, D. Noise and transport characterization of single molecular break junctions with individual molecule. *Journal of Applied Physics* **2012**, *112*, 014908.

[35] Wang, L.; Wang, L.; Zhang, L.; Xiang, D. Advance of Mechanically Controllable Break Junction for Molecular Electronics. *Topics in Current Chemistry* **2017**, *375*.

[36] Rubio, G.; Agrait, N.; Vieira, S. Atomic-sized metallic contacts: mechanical properties and electronic transport. *Physical Review Letters* **1996**, *76*, 2302.

[37] Agrait, N.; Rubio, G.; Vieira, S. Plastic deformation in nanometer scale contacts. *Langmuir* **1996**, *12*, 4505–4509.

[38] Rubio-Bollinger, G.; Bahn, S. R.; Agrait, N.; Jacobsen, K. W.; Vieira, S. Mechanical properties and formation mechanisms of a wire of single gold atoms. *Physical Review Letters* **2001**, *87*, 026101.

[39] Sørensen, M. R.; Brandbyge, M.; Jacobsen, K. W. Mechanical deformation of atomic-scale metallic contacts: structure and mechanisms. *Physical Review B* **1998**, *57*, 3283.

[40] Todorov, T.; Sutton, A. Force and conductance jumps in atomic-scale metallic contacts. *Physical Review B* **1996**, *54*, R14234.

[41] Cuevas, J.; Yeyati, A. L.; Martín-Rodero, A.; Bollinger, G. R.; Untiedt, C.; Agraït, N. Evolution of conducting channels in metallic atomic contacts under elastic deformation. *Physical Review Letters* **1998**, *81*, 2990.

[42] Torres, J.; Pascual, J.; Sáenz, J. Theory of conduction through narrow constrictions in a three-dimensional electron gas. *Physical Review B* **1994**, *49*, 16581.

[43] Li, C.; Sha, H.; Tao, N. Adsorbate effect on conductance quantization in metallic nanowires. *Physical Review B* **1998**, *58*, 6775.

[44] Torres, J.; Sáenz, J. Conductance and mechanical properties of atomic-size metallic contacts: a simple model. *Physical Review Letters* **1996**, *77*, 2245.

[45] López-Ciudad, T.; García-Martín, A.; Caamaño, A.; Sáenz, J. Conductance histograms and conducting channels in atomic-scale metallic contacts. *Surface Science* **1999**, *440*, L887–L890.

[46] Hansen, K.; Lægsgaard, E.; Stensgaard, I.; Besenbacher, F. Quantized conductance in relays. *Physical Review B* **1997**, *56*, 2208.

[47] Costa-Krämer, J. Conductance quantization at room temperature in magnetic and nonmagnetic metallic nanowires. *Physical Review B* **1997**, *55*, R4875.

[48] Costa-Krämer, J.; García, N.; Olin, H. Conductance quantization histograms of gold nanowires at 4 K. *Physical Review B* **1997**, *55*, 12910.

[49] Costa-Krämer, J.; García, N.; García-Mochales, P.; Serena, P.; Marqués, M.; Correia, A. Conductance quantization in nanowires formed between micro and macroscopic metallic electrodes. *Physical Review B* **1997**, *55*, 5416.

[50] Yuki, K.; Enomoto, A.; Sakai, A. Bias-dependence of the conductance of Au nanocontacts at 4 K. *Applied Surface Science* **2001**, *169*, 489–492.

[51] Muller, C.; Krans, J.; Todorov, T.; Reed, M. Quantization effects in the conductance of metallic contacts at room temperature. *Physical Review B* **1996**, *53*, 1022.

[52] Tsutsui, M.; Shoji, K.; Taniguchi, M.; Kawai, T. Formation and self-breaking mechanism of stable atom-sized junctions. *Nano letters* **2008**, *8*, 345–349.

[53] Alwan, M.; Candoni, N.; Dumas, P.; Klein, H. R. Statistical evidence of strain induced breaking of metallic point contacts. *The European Physical Journal B* **2013**, *86*, 243.

[54] Yang, Y.; Liu, J.-Y.; Chen, Z.-B.; Tian, J.-H.; Jin, X.; Liu, B.; Li, X.; Luo, Z.-Z.; Lu, M.; Yang, F.-Z.; Tao, N.; Tian, Z.-Q. Conductance histogram evolution of an EC–MCBJ fabricated Au atomic point contact. *Nanotechnology* **2011**, *22*, 275313.

[55] Yanson, A.; Bollinger, G. R.; Van den Brom, H.; Agrait, N.; Van Ruitenbeek, J. Formation and manipulation of a metallic wire of single gold atoms. *Nature* **1998**, *395*, 783.

[56] Ohnishi, H.; Kondo, Y.; Takayanagi, K. Quantized conductance through individual rows of suspended gold atoms. *Nature* **1998**, *395*, 780.

[57] Smit, R.; Untiedt, C.; Yanson, A.; Van Ruitenbeek, J. Common origin for surface reconstruction and the formation of chains of metal atoms. *Physical Review Letters* **2001**, *87*, 266102.

[58] Untiedt, C.; Yanson, A.; Grande, R.; Rubio-Bollinger, G.; Agraït, N.; Vieira, S.; Van Ruitenbeek, J. Calibration of the length of a chain of single gold atoms. *Physical Review B* **2002**, *66*, 085418.

[59] Dreher, M.; Pauly, F.; Heurich, J.; Cuevas, J. C.; Scheer, E.; Nielaba, P. Structure and conductance histogram of atomic-sized Au contacts. *Physical Review B* **2005**, *72*, 075435.

[60] Kizuka, T. Atomic configuration and mechanical and electrical properties of stable gold wires of single-atom width. *Physical Review B* **2008**, *77*.

[61] Pu, Q.; Leng, Y.; Cummings, P. T. Rate-dependent energy release mechanism of gold nanowires under elongation. *Journal of the American Chemical Society* **2008**, *130*, 17907–17912.

[62] Cortes-Huerto, R.; Sondon, T.; Saúl, A. Role of temperature in the formation and growth of gold monoatomic chains: A molecular dynamics study. *Physical Review B* **2013**, *88*, 235438.

[63] Yanson, A. Atomic Chains and Electronic Shells: Quantum Mechanisms for the Formation of Nanowires; *Universiteit Leiden*, **2001**.

[64] Ludoph, B.; Van Ruitenbeek, J. Conductance fluctuations as a tool for investigating the quantum modes in atomic-size metallic contacts. *Physical Review B* **2000**, *61*, 2273.

[65] Sirvent, C.; Rodrigo, J.; Vieira, S.; Jurczyszyn, L.; Mingo, N.; Flores, F. Conductance step for a single-atom contact in the scanning tunneling microscope: Noble and transition metals. *Physical Review B* **1996**, *53*, 16086.

[66] Oshima, H.; Miyano, K. Spin-dependent conductance quantization in nickel point contacts. *Applied Physics Letters* **1998**, *73*, 2203–2205.

[67] Scheer, E.; Joyez, P.; Esteve, D.; Urbina, C.; Devoret, M. H. Conduction channel transmissions of atomic-size aluminum contacts. *Physical Review Letters* **1997**, *78*, 3535.

[68] Yanson, A.; Van Ruitenbeek, J. Do histograms constitute a proof for conductance quantization? *Physical Review Letters* **1997**, *79*, 2157.

[69] Hasmy, A.; Medina, E.; Serena, P. From favorable atomic configurations to supershell structures: a new interpretation of conductance histograms. *Physical Review Letters* **2001**, *86*, 5574.

[70] Medina, E.; Díaz, M.; León, N.; Guerrero, C.; Hasmy, A.; Serena, P.; Costa-Krämer, J. Ionic shell and subshell structures in aluminum and gold nanocontacts. *Physical Review Letters* **2003**, *91*, 026802.

[71] Sáenz-Arce, G. Study of Atomic-Size Structures using a Scanning Tunneling Microscope with Force Resonant-Detection. Ph.D. thesis, **2011**.

[72] Delgado-Jiménez, L.; Chacón-Vargas, S.; Sabater-Piqueres, C.; Sáenz-Arce, G. Medidas topográficas en superficies atómicamente planas en condiciones ambiente mediante un microscopio de efecto túnel, un enfoque didáctico. *Uniciencia* **2019**, *33*, 30–42.

[73] Foley, E.; Candela, D.; Martini, K.; Tuominen, M. An undergraduate laboratory experiment on quantized conductance in nanocontacts. *American Journal of Physics* **1999**, *67*, 389–393.

[74] Huisman, E.; Bakker, F.; der Pal, J. v.; Jonge, R. d.; der Wal, C. v. Public exhibit for demonstrating the quantum of electrical conductance. *American Journal of Physics* **2011**, *79*, 856–860.